Determining Well Control Issues in HTHP Wells by Predicting Equivalent Circulating Density

By

Mohammad Adi Aiman Haji Sarbini
G01539

Dissertation submitted in partial fulfilment of
the requirements for the
MSc Petroleum Engineering
(MSc PE)

JULY 2012

Universiti Teknologi PETRONAS
32610 Bandar Seri Iskandar
Perak Darul Ridzuan

CERTIFICATION OF APPROVAL

Determining Well Control Issues in HTHP Wells by Predicting Equivalent Circulating Density

By

Mohammad Adi Aiman Haji Sarbini
G01539

A project dissertation submitted to the
Petroleum Engineering Programme
Universiti Teknologi PETRONAS
in partial fulfilment of the requirement for the
MSc of PETROLEUM ENGINEERING

Approved by,

_____

(Dr. Ismail M Saaid)

UNIVERSITI TEKNOLOGI PETRONAS
TRONOH, PERAK
JULY 2012

CERTIFICATION OF ORIGINALITY

This is to certify that I am responsible for the work submitted in this project, that the original work is my own except as specified in the references and acknowledgements, and that the original work contained herein have not been undertaken or done by unspecified sources or persons.

_____

Mohammad Adi Aiman Haji Sarbini

ACKNOWLEDGEMENTS

First of all I would like to express our gratitude to all those who has contributed in any way for the success of this Individual Project. I would like to take this opportunity to thank my direct supervisor of this project; Dr. Sonny Irawan. I am also deeply indebted to Pg. Amirrudin Pg. Hj. Razali (PetroleumBRUNEI), Hairol Nizam Mokti (PetroleumBRUNEI) for their guidance and useful suggestions which helped us in completing this project in time.

Finally, yet importantly, I would like to express our heartfelt thanks to our beloved family for their blessings, our friends and classmates for their help and wishes for the successful completion of this project.

ABSTRACT

Well control issues are caused mainly due to pressure instabilities in the wellbore. For example, when the hydrostatic pressure exerted by the mud column is being overcome by the pore pressure, the formation fluids start to invade the wellbore. This well control problem is also known as “kick”. Well control issues can also be caused when there is too much hydrostatic pressure exerted by the mud column which causes the formation to fracture. This formation fractures can mitigate, thus create a flow conduit in the formation where the drilling fluid can permeate and be lost – a common well control problem known as “lost circulation”. Furthermore, high temperature and high pressure formation normally has the issue of narrow bottomhole pressure margin between the pore pressure and the fracture pressure. This characteristic of the HTHP well means that there is a little margin for error when choosing the right mud weight and the mud components that can function properly within this margin. The problem is further complicated during circulation as the mud weight is increased depending on the amount of frictional pressure loss along the flow conduits, now defined as equivalent circulating density (ECD). Predicting the ECD requires circulating fluid temperatures to be simulated, which is built using implicit numerical methods by applying Crank-Nicolson solution. This temperature simulator is used in conjunction with the temperature and pressure dependent rheological properties of drilling fluids to evaluate the ECD. The results show that the bottomhole fluid temperature decreases with increasing circulation time and circulation rate, which consequently increase the ECD, which may lead to formation fracture. Furthermore, geothermal gradient is found to be the most sensitive parameter that may lead to well control problems if a linear gradient is assumed especially in heterogeneous HTHP formations. Therefore, choosing the right drilling fluid constituents that are stable in high temperature and high pressure, and compatible to be used in HTHP formation is critical to ensure well control issues are minimized.

SUMMARY

This project commenced officially on the 25th March 2012 and ended on the 22nd June 2012. During the first two weeks, literature reviews were being done from SPE journals as well as course notes, which consequently allowed me to develop clear objectives for this project. The following weeks were dedicated to develop the methodology, collecting data, developing mathematical models as well as simulating model to obtain results.

Building the model for temperature require the understanding of heat flow equations between the formation and inside the wellbore. Separate fluid temperature must also be taken into account for the fluid flowing down the drillpipe as well as up the annulus. The knowledge of fluid temperature profiles in both flow conduits allows the evaluation of ECD at the openhole. This requires a compositional model in order to predict the downhole density as a function of temperature and pressure. The evaluation of ECD also requires calculations of frictional pressure losses during fluid flow to be made. Two flow regimes could be considered to calculate this pressure loss i.e. laminar and turbulent flow. However, due to time constraints, an only pressure loss due to laminar flow was studied.

The prediction results show that during circulation, the fluid temperature at the openhole decreases with circulation time and circulation rate. This temperature reduction causes the density at that openhole to increase, thus, creating a fracture risk in HTHP formations, which have narrow pore and fracture pressure margins.

The biggest challenge in this project is to build a prediction model. This is where the majority of time was spent building such simulation model as it involved learning to program on Macro in Microsoft Excel that was able to numerically solve heat flow equations implicitly, and thus, predict circulating fluid temperature inside the wellbore.

Table of Contents

Table of Figures

List of Tables

Abbreviation

ECD	Equivalent Circulating Density
ESD	Equivalent Static Density
HTHP	High Temperature High Pressure
OBM	Oil-Based Mud
SBHP	Static Bottom Hole Pressure
UKCSON	United Kingdom Continental Shelf Operations Notice
WBM	Water-Based Mud

Nomenclature

A	surface area of drillpipe (in^2)
C_F	formation heat transfer coefficient (BTU/lb-°F)
C_{fl}	heat capacity of fluid (BTU/lb-°F)
d	pipe diameter (in)
d_1	inner annular wall (in)
d_2	outer annular wall (in)
F	force (N)
h	height of static drilling fluid (ft)
L	length of flow conduit (ft)
m	mass flow rate of fluid (gpm),
m_G	slope or geothermal gradient (°F/ft)
n	flow index (dimensionless),
ΔP_f	is the pressure loss due to friction
r_a	radius of the annulus (in),
r_d	radius of the drillpipe (in),
T_F	temperature in the formation (°F),
T_S	surface temperature (°F)
T_a	temperature in the annulus (°F),
T_d	temperature in the drillpipe (°F),
T_f	temperature of the formation (°F),
U_d	heat transfer coefficient between drillpipe and annulus (),
V_{oi}	volume of oil components in a drilling fluid
V_{wi}	volume of water components in a drilling fluid
V_{si}	volume of solids components in a drilling fluid
V_{ci}	volume of chemical components in a drilling fluid
z	depth (ft)
α	formation transmissivity ($^{k_F}/_{\rho C_F}$)
γ	shear rate
μ	consistency index (N/m^2s)

μ_a apparent fluid viscosity

$\mu_{p(T,P)}$ mud plastic viscosity at elevated temperature and pressure,

μ_{ps} mud plastic viscosity at surface conditions,

$\mu_{o(T,P)}$ base oil plastic viscosity at elevated temperature and pressure,

μ_{os} base oil plastic viscosity at surface conditions.

ρ fluid density (ppg)

ρ_F formation density (g/cm^3),

ρ_f new density of components subject to HTHP

ρ_{mi} mud density at reference condition

ρ_{mf} mud density at elevated temperature and pressure

ρ_{oi} oil density at reference conditions

ρ_{of} oil density at elevated temperature and pressure

ρ_{wi} water density at reference conditions

ρ_{wf} water density at elevated temperature and pressure

τ shear stress,

τ_y fluid yield point (N/m^2)

τ_{y0} yield point at surface conditions (N/m^2)

f fanning friction factor,

f_o volume fractions of oil and water

f_w volume fractions of oil and water

k_F formation conductivity

v fluid velocity (m^3/s),

$\bar{v}$ average flow velocity (m^3/s),

CHAPTER 1
INTRODUCTION

1.1 Problem Statements

High temperature, high pressure (HTHP) formation presents a challenge while drilling a well. These challenges include how HTHP conditions affect normal drilling operations and the problems they pose to the stability of the wellbore.

The hydrostatic pressure of the fluid column in a borehole depends on the mud density and this is different from that on the surface due to the increasing temperature and pressure with depth. Mud density in the wellbore very well depends on its rheology, which is also affected by temperature and pressure. While circulating the drilling fluid, pressure losses are expected, which determine the Equivalent Circulating Density (ECD). The problem is that mud density and ECD change with temperature and pressure, and this change alter the behaviour of the drilling fluid, which consequently affects the wellbore stability and drilling operations, especially in HTHP wells. Therefore, by predicting ECD, is it possible to predict wellbore issues?

1.2 Objectives

The main objectives of this project are as follows:

1. To determine the effects of HTHP conditions on the physical and chemical properties of drilling fluids such as density and rheology
2. To evaluate the impact of these altered properties of drilling fluids (due to HTHP conditions) on wellbore stability or well control issues
3. To develop a mathematical model to predict:
    a. Formation temperature
    b. Circulating drilling fluid temperature
    c. Equivalent circulating density

1.3 Scope of Study

The scope of study in this project involves the geology and the formation of high temperature, high pressure (HTHP) wells. This subject includes the classifications of these wells and their distinctive features. The study will also cover drilling engineering subject, which envelopes related topics to this project such as drilling fluids, well control and hydraulics. In hydraulics, the flow properties as well as rheological models will also be studied.

Heat transfer will also be examined in order to understand how heat energy flow from one medium to another. This will allow the development of a mathematical model to predict this heat exchange between the formation and the downhole drilling fluids, which eventually leads to the development of a simulation model to predict both the bottomhole fluids temperatures as well as the equivalent circulating density.

This will involve the numerical simulation studies using finite difference techniques and solutions compared between explicit and implicit methods. Several other methods will also be discussed that would make the numerical simulation more accurate and efficient such as the Crank-Nicolson and Thomas algorithm.

1.4 Data Availability

Data is made available to be used in this project from an HTHP well in Brunei, Berambang-1 well. Such data include:

- Pore-fracture pressure plot
- Temperature gradient
- Daily drilling and geological reports

1.5 Project Schedule & Organization

Figure 10.1 in the Appendix shows the project schedule.

CHAPTER 2
LITERATURE REVIEW

2.1 Geothermal Gradients

Geothermal gradient is defined as the amount of temperature increase with depth in the earth's crust, and is usually expressed in the form of °F/100ft (°C/km). According to Caenn et al 2011 [**1**], there are two main sources of heat flow in the upper crust;

1. Heat conduction from the lower crust and mantle
2. Heat produced from radioactive decay in the upper crust

Geothermal gradients vary from place to place depending on a number of factors such as (Caenn *et al* 2011 [**1**]):

- The amount of heat produced by radioactive decay in the upper crust
- Structural features
- Thermal conductivity of the formation; high gradients in low conductivity zone such as shale and low gradients in high conductivity zones such as sandstone
- Convection flow; for thick permeable formation, water circulates by convection which creates high temperature at shallow depths
- Pore pressure profiles; geopressured formations have higher temperature gradients

Due to these factors, geothermal gradients have different ranges around the world, for example, 0.44°F/100ft to 2.7°F/100ft in the United States, and 1.2°F/100ft to 2.2°F.100ft in the Gulf Coast. Steam wells in California have geothermal gradients as high as 12.5°F/100ft due to water circulating via convection. One finding from detailed surveys is that geothermal gradients are not linear with depth but depends on the factors listed above.

2.2 High Temperature High Pressure

United Kingdom Continental Shelf Operations Notice (UKCSON) has defined a High Temperature, High Pressure (HTHP) as any well that has:

- A bottomhole temperature starting from 150°C (300°F), or
- Pore pressure exceeding 0.8 psi/ft
- A bottomhole pressure beyond 10,000 psi

2.2.1 Classifications

Schlumberger (DeBruijn *et al* 2008 [**2**]) has classified HTHP formations into three distinct groups;

1. HTHP
2. Ultra HTHP
3. Extreme HTHP

HTHP wells are identified as those with a minimum bottomhole temperature of 150°C (300°F) or bottomhole pressure of 10,000 psi. For higher bottomhole temperature of 205°C (400°F) or bottomhole pressure of 20,000 psi, these wells are called as Ultra HTHP. Finally, Extreme HTHP wells have bottomhole temperatures beyond 260°C (500°F) or bottomhole pressure of 35,000 psi. Figure 2.1 illustrates the classification of HTHP wells with their respective pressures and temperatures.

The boundaries between the HTHP classifications represent stability limits of common tools and components, especially elastomeric seals and electronic components.

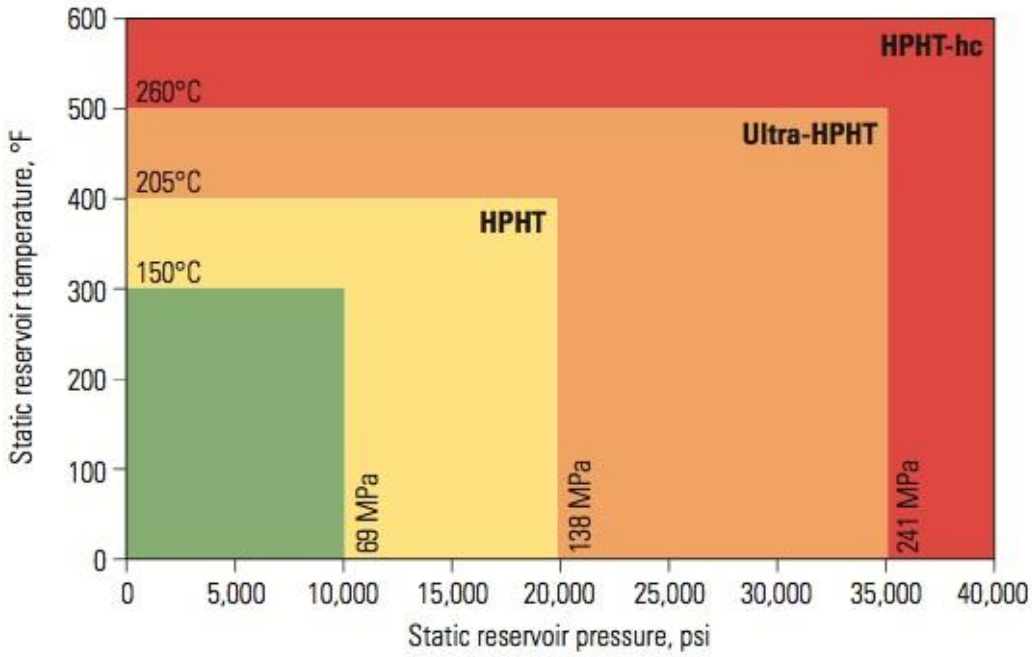

Figure 2.1: Schlumberger classification of HTHP formations (DeBruijn *et al* 2008 [2])

2.2.2 Characteristics of HTHP Wells

Other than using the classification shown in Figure 2.1, HTHP wells can be easily identified by looking at the pore pressure and fracture pressure gradients plot, where a narrow margin is expected between the pore pressure and fracture pressure about the bottomhole.

2.3 Properties of Drilling Fluids

2.3.1 Functions

The primary functions of drilling fluids are listed in the following (Caenn *et al* 2011 [**1**]):

1. Carry cuttings from the bottomhole up to the surface through the annulus
2. Cool and clean the drillbits
3. As a lubricant to reduce friction between drillstring and walls of annulus or formation
4. Exert hydrostatic pressure on the wellbore to prevent from collapsing

5. Forms filter cake along the borehole wall to prevent formation fluids from entering the borehole

2.3.2 Composition

Drilling fluids are identified according to their base fluid, which are; aqueuous, non-aqueous or gas.

Aqueuous

In water-based (brine) muds, solid particles are suspended which consist of clays, organic colloids, heavy minerals as well as drill cuttings. These additives provide the necessary mud properties such as viscosity and filtration properties as well as density, which aid the abilities of the drilling fluids.

Water-based muds are often composed of bentonite clay, which becomes unstable with increasing temperatures. This is because at high temperature the adsorbed water layer of the bentonite clay changes in its orientation (Fisk 1989 [**3**]).

Non-aqueous

Non-aqueous type can be oil-based, synthetic or invert emulsion.

Oil-based muds often contain organic clay compounds which allow the formation of gel-like structure. The physical properties of these organophillic clay do not change very much with increasing temperature as compared to bentonite clay.

Gas

High-velocity stream of air or nitrogen aids the evacuation of drill cuttings.

2.3.3 Physical Properties

The physical properties of drilling fluids are controlled by adding additives (Fisk 1989 [**3**]). What these additives do is that they create enough solid-solid and solid-

liquid interactions to form gels and filter cakes, which are needed for a drilling fluid to carry out its functions such as, suspend solids, control fluid invasion into the formation as well as prevent inflow of formation fluids.

2.3.4 Density

Density is defined as mass over volume. The volume term can be influenced by temperature and pressure. Increasing temperature causes thermal expansion, and this increase in volume causes the density to decrease. Increasing pressure, however, decreases the volume, which consequently cause the density to increase.

The hydrostatic pressure of the fluid column in a borehole depends on the mud density, which is different from that on the surface due to the increasing temperature and pressure with depth. This hydrostatic pressure must exceed the pore pressure in the formation. If the hydrostatic pressure is less than the pore pressure, this will incite the inflow of formation fluids into the wellbore which may potentially cause a blowout and the wellbore may even collapse.

At the same time, the hydrostatic pressure of the fluid must also not exceed the fracture pressure of the formation. Excessive mud density may induce formation fracturing, which may potentially pose more well control problems.

Therefore, the density of the drilling mud must be examined carefully so that it exerts a sufficient hydrostatic pressure that lies in between the pore pressure and fracture pressure.

2.3.5 Flow Regimes

With the right flow regime, drill cuttings can be removed successfully and efficiently as well as influence the drilling operations. Failure to do so can lead to serious well issues such as hole bridging, barite sagging, reduced penetration rates, hole caving, stuck pipe, lost circulation and worse, blowouts. Hence, the flow properties of the drilling fluid play a vital role to ensure successful drilling operations.

There are two flow regimes; laminar flow and turbulent flow.

Laminar Flow

Laminar flow (streamline or viscous flow) basically occurs at low velocity and it is a function of the viscosity. Layers of fluid move in streamlines or laminae. Figure 2.2 illustrates the flow behaviour of this viscous flow.

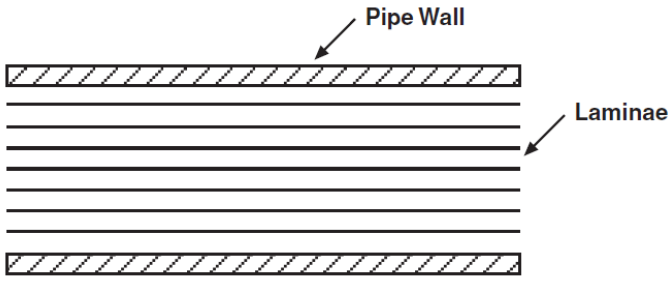

Figure 2.2: Illustration of laminar flow inside a drillpipe (Heriot-Watt University 2005 [4])

Turbulent Flow

Turbulent flow occurs at high flow velocity, which is governed by the inertial properties and indirectly influenced by the viscous properties of the drilling fluid. This flow is illustrated in Figure 2.3.

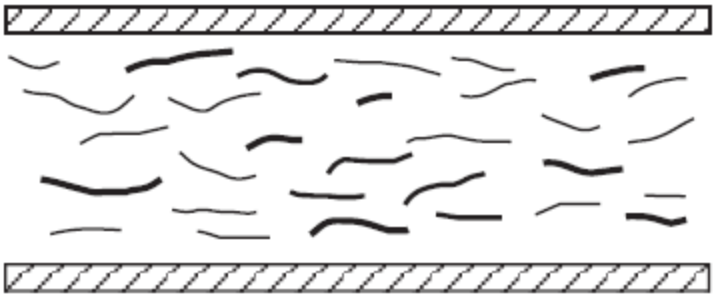

Figure 2.3: Illustration of turbulent flow inside a drillpipe (Heriot-Watt University 2005 [4])

Determination of Flow Regime

Figure 2.4 shows the relationship between laminar flow and turbulent flow. These two flow regimes can be determined by using Reynolds number. Circulating fluids through pipes is a function of pipe diameter, fluid density, viscosity and average flow velocity, as shown in the following equation (Heriot-Watt University 2005 [**4**]),

$$N_{RE} = \frac{928\rho\bar{v}d}{\mu_a} \tag{2.1}$$

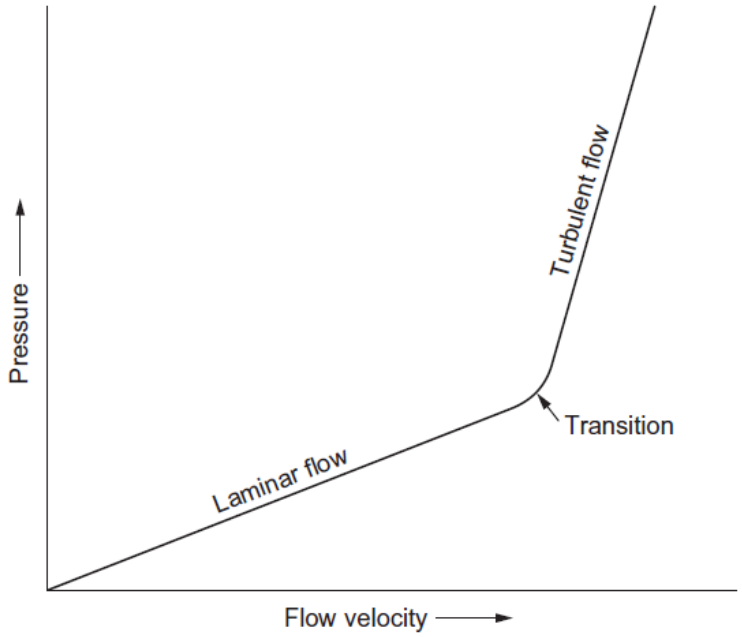

Figure 2.4: Relationship between laminar flow and turbulent flow (Caenn et al 2011 [1])

As the fluid velocity is increased, the flow pattern changes from laminar to turbulent flow and this occur at a Reynolds number of 2100 for Newtonian fluids.

2.3.6 Rheology Models

Rheology is the study of the deformation and flow of matter (Caenn *et al* 2011 [**1**]). A viscous force relationship can be developed to describe a simple rheology model from Figure 2.5 below.

$$\frac{F}{A} = \mu\frac{V}{L} \tag{2.2}$$

The term F/A is called shear stress, τ, while V/L is the shear rate, γ.

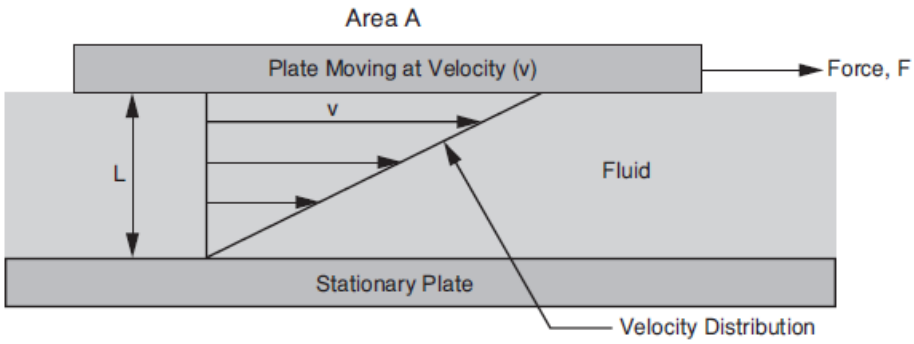

Figure 2.5: Model of Viscous Forces in Fluids (Heriot-Watt University 2005 [4])

Bingham Plastic Model

The equation for Bingham Plastic model can be expressed in the following equation (ASME 2004 [**5**]),

$$\tau = \mu\gamma + \tau_y \tag{2.3}$$

Power Law Model

Power Law can be expressed mathematically as follows (ASME 2004 [**5**]),

$$\tau = \mu\gamma^n \tag{2.4}$$

Herschel-Bulkley Rheological Model

Herschel-Bulkley (H-B) is widely applied in industrial standards. There are three parameters required in this model, expressed in the following equation (ASME 2004 [**5**]),

$$\tau = \mu\gamma^n + \tau_y \tag{2.5}$$

H-B is essentially a hybrid between the Power Law and Bingham Plastic models. When the yield stress, τ_y, is equal to the yield stress, the flow index, $n = 1$, which reduces the H-B model equation to the Bingham Plastic model. Inversely, when the yield stress is zero, $\tau_y = 0$, the H-B then becomes the Power Law. Figure 2.6 shows

the comparison between Bingham Plastic, Power Law, Newtonian and Herschel-Bulkley (ideal power law) rheological models.

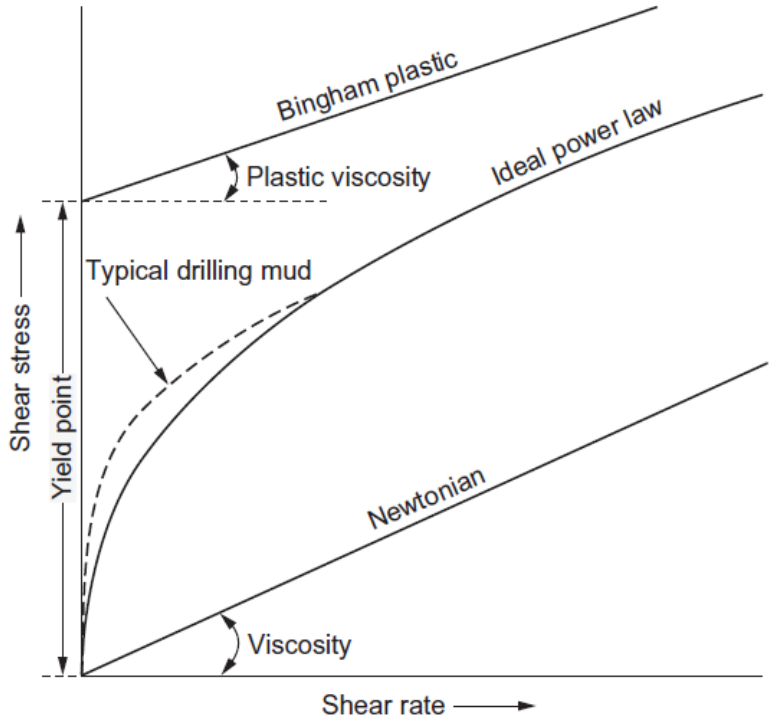

Figure 2.6: Comparison between different rheological models (Caenn *et al* 2011 [1])

Consistency index parameter, k, is equivalent to the Plastic Viscosity term in the Bingham Plastic rheological model. Fluid yield stress parameter, τ_y, is equivalent to the yield point in the Bingham Plastic model, which describes the suspension behavior of drilling mud. However, the actual value of yield stress can only be obtained from field viscometer measurements or numerical methods.

Another way to describe H-B model is that it is essentially a Power Law with a yield stress.

2.4 Equivalent Circulating Density

2.4.1 Equivalent Static Density

Equivalent Static Density (ESD) is equivalent to the hydrostatic pressure exerted at any point by a column of fluid and it is a function of the fluid density and the height

of the fluid column. ESD can be mathematically expressed by the following equation (Harris *et al* 2005 [**6**]),

$$\rho_{ESD} = \frac{\text{SBHP}}{0.052h} \tag{2.6}$$

2.4.2 Frictional Pressure Loss

Frictional pressure loss is due to contact between the drilling fluid and the walls of conduit flow i.e. annulus and drill string. This pressure loss can be expressed by the following equation (Harris *et al* 2005 [**6**]),

$$\Delta P_f = \frac{2f\rho v^2}{d}\Delta L \tag{2.7}$$

2.4.3 Equivalent Circulating Density

Equivalent Circulating Density (ECD) at the total depth is defined as the sum of the ESD and the pressure loss in the annulus due to fluid flow. ECD is equivalent to the bottomhole pressure equation expressed as a drilling fluid-density gradient as follows:

$$\rho_{ECD} = \rho_{ESD} + \frac{\Delta P_{friction}}{0.052h} \tag{2.8}$$

2.5 Review of Finite Difference Scheme

According to Heriot-Watt University 2005 [**7**], finite difference technique is essentially a simple method to approximate derivatives of a function numerically from either point, node or block values of the function, such as, $\left(\frac{dP}{dx}\right)$, $\left(\frac{\partial P}{\partial t}\right)$, $\left(\frac{\partial^2 P}{\partial x^2}\right)$, etc.

Figure 2.7 below illustrates the concept of finite difference graphically, which an average between a forward difference and a backward difference can be done to obtain a more accurate approximation.

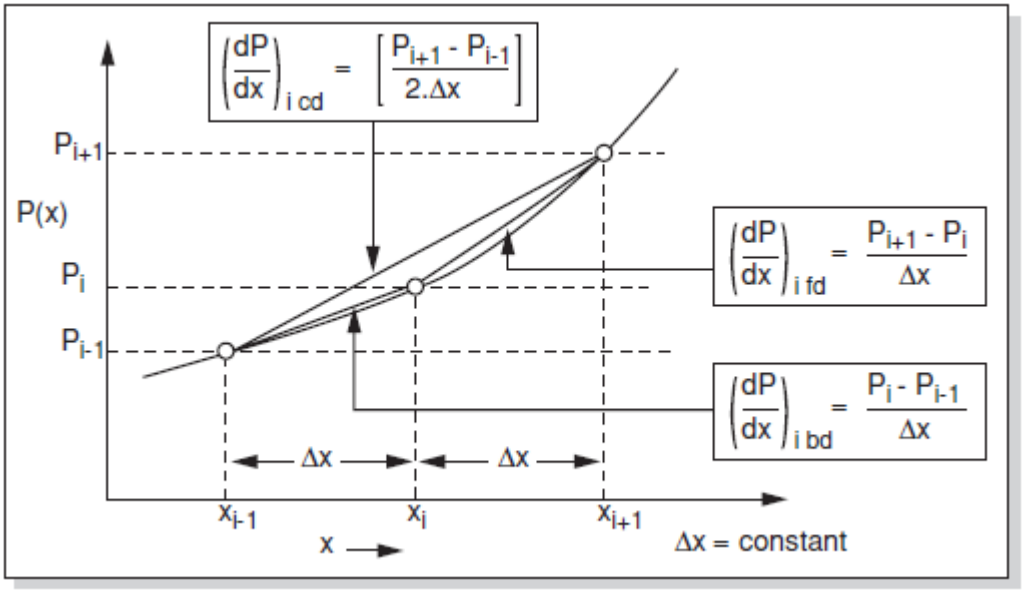

Figure 2.7: Graphical representation of the finite difference derivatives calculated using forward difference, backward difference and central difference. (Heriot-Watt University 2005 [7])

Forward difference

Forward difference is basically the gradient between P_i and P_{i+1}, which is approximated at x_i, as represented by the following (Heriot-Watt University 2005 [**7**]),

$$\left(\frac{dP}{dx}\right)_{i,fd} = \frac{P_{i+1} - P_i}{\Delta x} \tag{2.9}$$

Backward difference

Similarly, backward difference is described as the slope taken between P_{i-1} and P_i, which is also approximated at x_i, as follows (Heriot-Watt University 2005 [**7**]),

$$\left(\frac{dP}{dx}\right)_{i,bd} = \frac{P_i - P_{i-1}}{\Delta x} \tag{2.10}$$

Central difference

From each of the two finite difference methods, approximations can be made, which, however, introduce an error from the true values. This error can be further reduced by introducing a Central Difference method, which is basically taking an average between the two slopes i.e. forward difference and backward difference. This is expressed by the following (Heriot-Watt University [**7**]),

$$\begin{aligned}\left(\frac{dP}{dx}\right)_{i,cd} &= \frac{1}{2}\left[\left(\frac{dP}{dx}\right)_{i,fd} + \left(\frac{dP}{dx}\right)_{i,bd}\right] \\ &= \frac{1}{2}\left[\frac{P_{i+1} - P_i}{\Delta x} + \frac{P_i - P_{i-1}}{\Delta x}\right] \\ &= \left[\frac{P_{i+1} - P_{i-1}}{2\Delta x}\right]\end{aligned} \tag{2.11}$$

Now that we have derived finite difference for the first derivative, then according to Heriot-Watt University 2005 [**7**], using the same technique, the second derivative can be formulated as follows,

$$\begin{aligned}\left(\frac{d^2P}{dx^2}\right) &= \frac{\left(\frac{dP}{dx}\right)_{i,fd} - \left(\frac{dP}{dx}\right)_{i,bd}}{\Delta x} \\ &= \frac{\frac{P_{i+1}-P_i}{\Delta x} - \frac{P_i-P_{i-1}}{\Delta x}}{\Delta x} \\ &= \frac{P_{i+1} - 2P_i + P_{i-1}}{(\Delta x)^2}\end{aligned} \tag{2.12}$$

There are two ways to solve a finite difference problem, which are explicit method and implicit method. These are explained briefly in the following subsections.

2.5.1 Explicit Solution

Explicit method is one of the techniques to solve a finite difference problem. By taking a simplified equation as follows,

$$\left(\frac{\partial P}{\partial t}\right) = \left(\frac{\partial^2 P}{\partial x^2}\right) \tag{2.13}$$

This finite difference problem is being approached as follows:

- The x-direction is discretize by dividing it into a numerical grid of size Δx
- A time step is chosen, Δt,
- The notation in P_i^n represent the following;
    - n is the time level, $n = 0, 1, 2$ ...

      i is the x-grid block label, $i = 1, 2, 3$ ...

Essentially, P_i^n is the current and known value of P at a time level, whilst P_i^{n+1} is the new and unknown value at another time level.

In order for this problem to be solved, boundary conditions must first be fixed such as the initial conditions, size of the grid block, etc.

Now by applying finite difference from Equation 2.9 (forward difference) and Equation 2.12, equating the expressions results the following,

$$\left(\frac{\partial P}{\partial t}\right)_i \approx \left(\frac{\partial^2 P}{\partial x^2}\right)_i$$

$$\frac{P_i^{n+1} - P_i^n}{\Delta t} \approx \frac{P_{i+1}^n - 2P_i^n + P_{i-1}^n}{(\Delta x)^2} \tag{2.14}$$

Now we can rearrange Equation 2.14 to obtain an explicit expression for the only unknown in the equation, P_i^{n+1},

$$P_i^{n+1} = P_i^n + \frac{\Delta t}{(\Delta x)^2}(P_{i+1}^n - 2P_i^n + P_{i-1}^n) \quad (2.15)$$

Equation 2.15 can be illustrated by the following diagram,

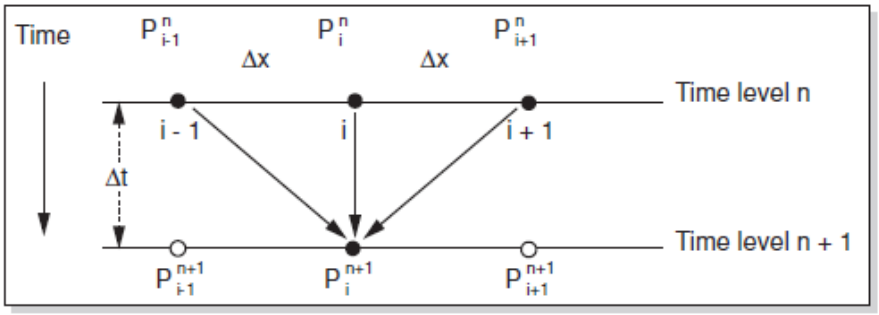

Figure 2.8: Schematic of explicit finite difference algorithm for solving simple partial differential equation (Heriot-Watt University 2005 [7])

There are several limitations when using explicit method to do approximations such as:

- If the time step Δt is too big, the numerical solution can become unstable.
- The accuracy of the approximation depends on how small the grid is (Δx). The smaller the grid, the longer it takes to run the calculations.

2.5.2 Implicit Solution

Implicit method is another technique to solve the finite difference problem, which takes the derivative of function at the (n+1) time level, which is the unknown time level. By taking the same expression as in Equation 2.13, the temporal term remains the same,

$$\left(\frac{\partial P}{\partial t}\right)_i = \frac{P_i^{n+1} - P_i^n}{\Delta t}$$

But the spatial terms are at the new time levels as follows,

$$\left(\frac{\partial^2 P}{\partial x^2}\right)_i = \frac{P_{i+1}^{n+1} - 2P_i^{n+1} + P_{i-1}^{n+1}}{(\Delta x)^2} \tag{2.16}$$

By equating these two equations to obtain the following (Heriot-Watt University 2005 [7]),

$$\frac{P_i^{n+1} - P_i^n}{\Delta t} = \frac{P_{i+1}^{n+1} - 2P_i^{n+1} + P_{i-1}^{n+1}}{(\Delta x)^2} \tag{2.17}$$

Now, rearranging Equation 2.17 such that all the unknown terms are on one side (LHS) while the only known term (RHS) on the other side of the equation. This is shown below,

$$P_{i+1}^{n+1} - \left[2 + \frac{(\Delta x)^2}{\Delta t}\right] P_i^{n+1} + P_{i-1}^{n+1} = -\left[\frac{(\Delta x)^2}{\Delta t}\right] P_i^n \tag{2.18}$$

This equation can be written as follows,

$$a_{i+1} P_{i+1}^{n+1} + a_i P_i^{n+1} + a_{i-1} P_{i-1}^{n+1} = b_i \tag{2.19}$$

Where,

$a_{i+1} = 1$

$a_i = -\left[2 + \frac{(\Delta x)^2}{\Delta t}\right]$

$a_{i-1} = 1$

$b_i = -\left[\frac{(\Delta x)^2}{\Delta t}\right] P_i^n$

As the new time level P^{n+1} is calculated and set to P^n, the values of a_i do not change while b_i is updated at each time step. This can be illustrated by taking a 5 grid block system as shown in Figure 2.9 below,

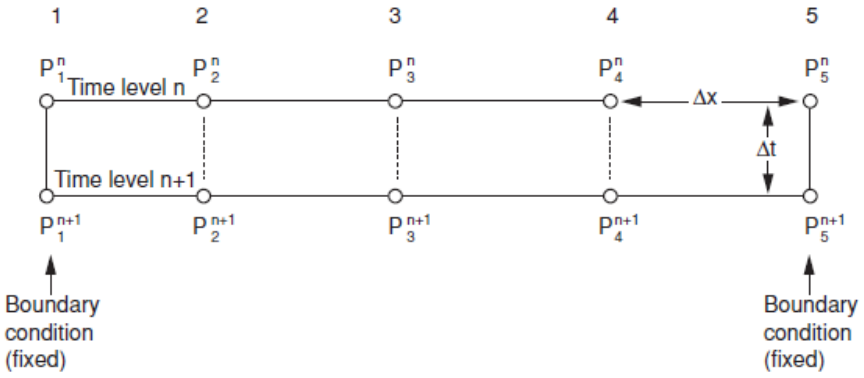

Figure 2.9: A 5 grid block system showing how implicit finite difference scheme works. (Heriot-Watt University [7])

The illustration of Equation 2.18 is shown in the diagram below.

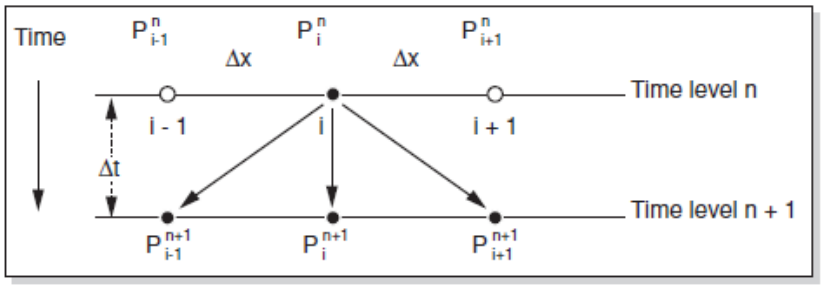

Figure 2.10: Schematic of explicit finite difference algorithm for solving simple partial differential equation (Heriot-Watt University 2005 [7])

CHAPTER 3
METHODOLOGY

3.1 Overall

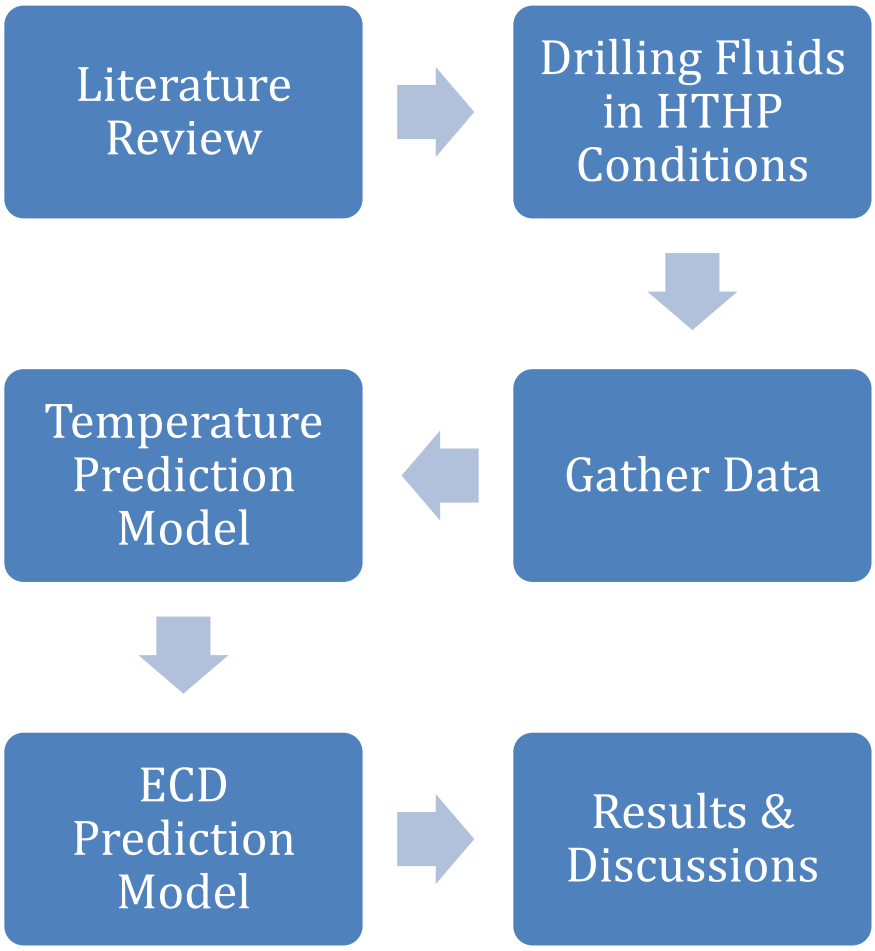

Figure 3.1: Methodology outline

3.2 Drilling Fluids in HTHP Conditions

The behaviour of drilling fluids at elevated temperature and pressure are to be studied and compared with normal formation, especially on how these conditions influence the mud density, mud temperature as well as the mud rheology that can have impact on the borehole stability.

3.3 Temperature Estimation

Mud temperature profile varies depending on the drilling parameters and circulation history. In order to establish temperature profiles at different pump rates and times from the start of circulation, a temperature simulator is required which involves discretization process in order to solve solutions numerically. Once simulated, the data generated can then by applied in the hydraulics calculations, which allows the prediction of static pressure element at circulating temperature profiles.

The temperature simulator must be able to generate the temperature profiles of the following:

- Formation temperature
- Fluid temperature in annulus
- Fluid temperature in drillstring
- How the temperature profile changes with time,

The temperature profiles in the annulus and drillstring have to be evaluated separately to take into account the heat transfer from the formation to the drilling fluids in the annulus, which is different from the mud temperature inside the drillstring. Furthermore, these temperature profiles are dynamic as they vary with time until equilibrium is reached.

From the geothermal gradient given from the Berambang-1 well data, along with other data, this would allow the temperature profile to be plotted against depth.

There are two approaches in estimating the circulating fluid temperatures; analytical and numerical.

Below is the list of approach to establish the wellbore temperature model:

- Introduce heat flow equations
- Establish heat flow diagram in the wellbore
- Derive analytical solutions
- Develop numerical solutions using finite difference techniques

3.3.1 Analytical Approach

The analytical approach involves the derivation of heat flow equations inside the wellbore between the drillpipe, annulus and the formation.

3.3.2 Numerical Solutions

The numerical approach involves the application of finite-difference technique in order to solve the transient heat transfer problem as proposed by Raymond 1969 [**8**], using the analytical solutions derived. Boundary conditions must also be set initially. Crank-Nicolson implicit solution will also be looked into.

3.4 ECD Model

The development of the ECD model will require in-depth study of the drilling fluids and their rheological properties. The methodology involved building this ECD prediction model firstly involves the prediction of downhole temperature and pressure dependent base mud densities using empirical equations. Then, a compositional model is used to obtain the density of mud at elevated temperature and pressure.

The next step is to look into how rheological properties change with temperature and pressure, where plastic viscosities and yield points at elevated conditions are calculated using the densities obtained from the compositional model. From these rheological properties calculations, the frictional pressure loss can be evaluated, depending on whether the flow is laminar or turbulent.

Once the frictional pressure loss is obtained, the ECD can now be evaluated. Sensitivity analysis can be made afterwards to see how the input parameters vary and which of them is the most sensitive.

CHAPTER 4
DRILLING FLUIDS IN HTHP CONDITIONS

4.1 Influence on Mud Temperature

The bottomhole temperatures of drilling wells are always less than the formation temperature due to the cooling effects of drilling fluid as it circulates around the borehole and the surface. Once the circulation is stopped, a rise in temperature can be expected downhole as seen in Figure 4.1 below [**8**]. Note that not the entire borehole experiences an increase in temperature with time; only the bottom half part of the well whilst the rest of the well up to the surface undergoes heat transfer to the formation, hence, a decrease in mud temperature with time.

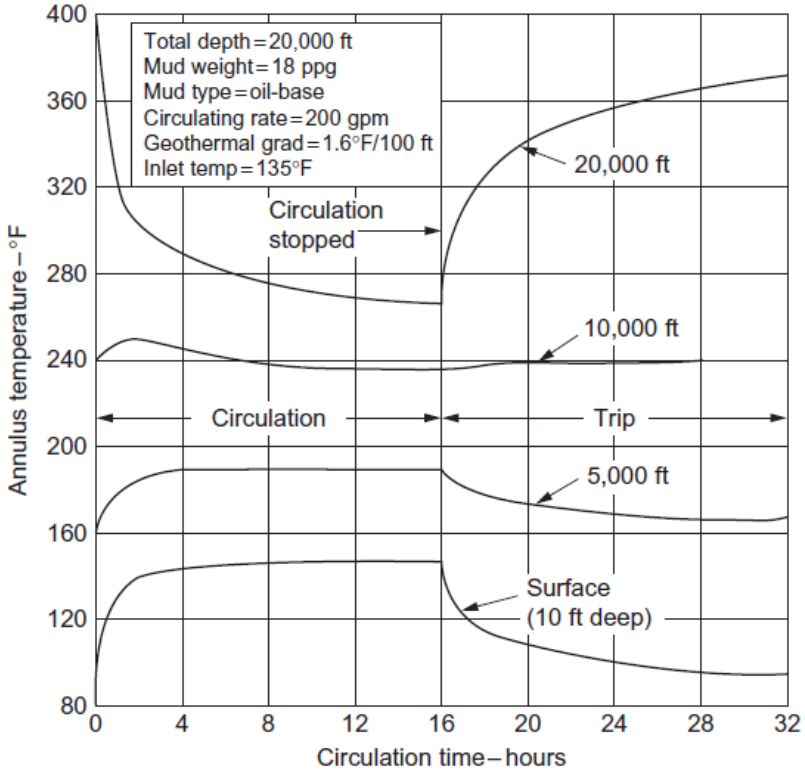

Figure 4.1: Temperature trace for various depths in a simulated well (Caenn *et al* 2011 [1])

4.2 Influence on Mud Density

According to Caenn *et al* 2011 [**1**], an experiment was conducted to see the effects of density with temperature and pressure using fresh-water bentonite mud and a low

viscosity oil mud. The results are shown in Figure 4.2, where a reduction in density can be seen with increasing temperature. The increase in pressure, however, increases the density.

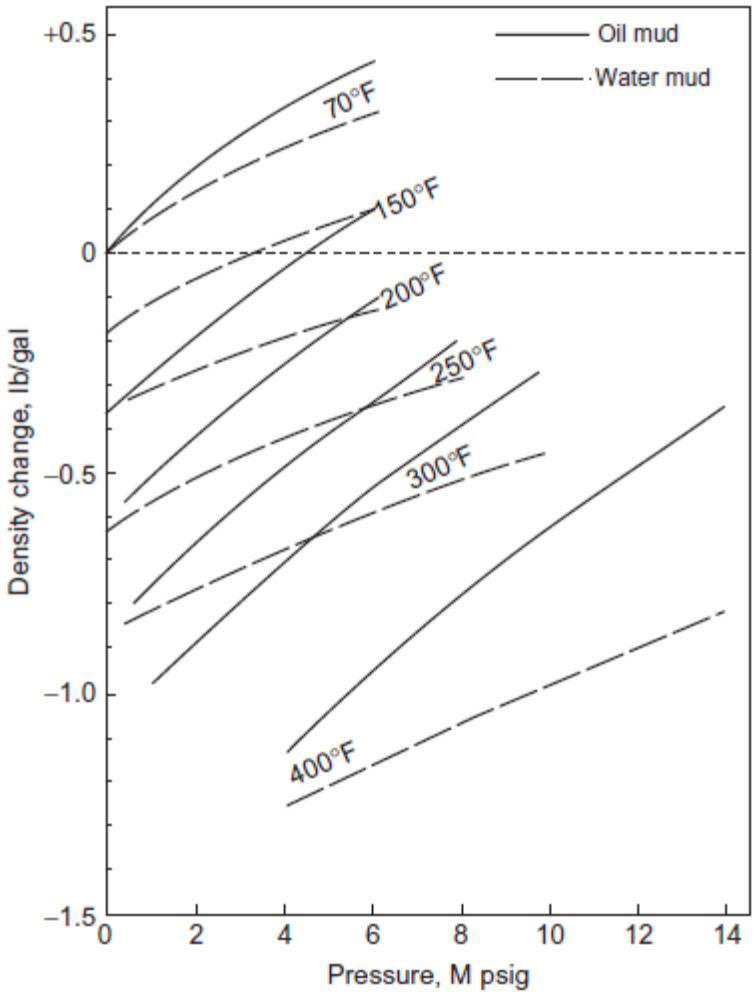

Figure 4.2: Effect of temperature and pressure on the density of oil-based and water-based drilling fluids (Caenn *et al* 2011 [1])

4.3 Influence on Rheology

High temperature and high pressure conditions change the rheological properties of drilling fluids. According to Rommetveit and Bjørkevoll 1997 [**9**], the rheological properties of drilling fluids are normally independent of temperature and pressure. This is because for normally pressured wells, the temperature variation is small so it does not significantly affect the mud rheology.

HTHP conditions can influence the rheological properties of drilling fluids any of the following ways (Caenn et al 2011 [**1**]):

4.3.1 Physical properties

The viscosity of the drilling fluid reduces as the temperature is increased. Conversely, increase in pressure results in the increase in mud density, thus increases the viscosity.

4.3.2 Chemical properties

Alkalinity levels in drilling fluids play some roles in how their rheological properties change with temperature and pressure. All hydroxides react with clay minerals at temperatures above 94°C (200°F). Low alkalinity muds have minimal impact on its rheological properties, unlike high alkalinity muds, which may have severe effects.

4.3.3 Electrochemical properties

An increase in temperature increases the ionic activity of any electrolyte and the solubility of any partially soluble salts that may be present in the mud. Changes in the ionic activities affect the degree of dispersion or flocculation, which consequently affects the rheology of mud.

The effect of water-based muds at high pressure and high temperature were studied. The findings were such that if a suspension is completely deflocculated, the plastic viscosity and yield point decrease with temperature up to 177°C (350°F). For a deflocculated mud, however, the yield point increases rapidly once the temperature exceeds boiling point of water while the plastic viscosity remains declining.

4.4 Critical Temperature

The issue with high temperature formations is that the constituents of drilling fluids degrade with time at these elevated conditions. The rate of degradation is directly proportional to temperature, therefore, this relationship must be taken into account

when selecting the constituents of a drilling mud. These degraded components can be replaced, but there is a point when the cost of replacing the materials becomes uneconomical, which is called the critical temperature. The table below shows the critical temperatures for several mud components (Caenn *et al* 2011 [**1**]);

Table 4.1: Critical temperatures for several muds and mud components

Materials/muds	**Critical Temperature,** °F
Starch	225
Cellulosic polymers	275
CL-CLS muds	350
Invert emulsions	400
Asphaltic oil muds	550
Polyacrylates	400
Acrylic copolymers	500

4.5 Rheology Experiments

Rheology experiments were conducted by Rommetveit and Bjørkevoll 1997 [**9**] to see the dependency of drilling fluids on high temperature and high pressure conditions. Fann 70 viscometer was used with 16 different HTHP drilling fluids being used. The conditions of the experiments are tabulated in below.

Table 4.2: Conditions applied during rheology experiments

Parameters	**Values**
Temperature	Up to 200°C (400 °F)
Pressure	Up to 1200 bar (17,500 psi)
Circulation rates	3-600 rpm

The findings from the experiments can be divided into two; the first part is where the rheological properties do not change with time, and secondly where these properties change dependent on time.

4.5.1 Time-independent properties

- Increase in temperature from 50-150°C (122-302°F), the shear stress for a high shear rate reduces significantly.
    - Beyond 150°C (302°F), the shear stress increases with increasing temperature.
- For temperature below 140°C (284°F), the shear stress for a low shear rate has less dependency on pressure and temperature.
    - Temperature 140-200°C (284-392°F), the shear stress increases rapidly.
- Pressure dependence is more significant with oil-based muds (OBM) compared to water-based muds (WBM).
    - For OBM, pressure and temperature effects almost cancelled each other out.
    - For WBM, temperature has a more significant impact than pressure.

4.5.2 Time-dependent properties

Over time, high temperature and high pressure significantly increases the gel strength of the mud.

4.6 Limitations

There are limitations with using conventional drilling fluids in HTHP wells, which is described in the following list (Godwin *et al* 2011 [**10**]):

- High ECD due to high loading of barite which creates high frictional pressure losses during circulation in long sections.
- The ability of drilling fluids to carry solids degrades at high temperature, resulting dynamic and static barite sag.
- Oil-based muds may absorb large volume of gas, and if the gas is hydrocarbon, it can cause instability in the mud formulation, which may lead to well control issues.

Recent HTHP wells have been utilizing invert emulsion drilling fluids which can accommodate temperatures up to 315°C (600°F) (Godwin *et al* 2011 [**10**]).

Thinning agents may be added into the mud formulation in order to control the increase in yield point with temperature, but these additives also degrade with temperature. Of course, they can be replaced from time to time but as the rate of degradation increases, and so as the cost.

CHAPTER 5
TEMPERATURE PREDICTION MODEL

As discussed previously, it is necessary to predict the temperature profile in the wellbore as high temperature have implications on the volumetric and rheological properties of the drilling fluids. In a HTHP well, flowing mud in the annulus absorbs heat from the formation via conduction, resulting an increase in its temperature.

The determination of mud temperature profile in the drillpipe and annulus involves the analysis of heat flow in the wellbore.

Firstly, the temperature profile of the formation needs to be simulated using the given data i.e. geothermal gradient and surface temperature.

5.1 Geothermal Gradient

Modeling the formation's geothermal gradient is a straight-forward process, using the available data, which is usually given in the information of the field being investigated. The geothermal gradient may be given in units of °F per 100ft, °F/ft, or °C/m. It may also be given in the form of a linear equation with an intercept such as the following,

$$T_F = m_G z + T_S \tag{5.1}$$

Where,

T_F is the temperature in the formation (°F),

m_G is the slope or geothermal gradient (°F/ft)

z is the depth (ft or m)

T_S is the surface temperature (°F)

The geothermal gradient is assumed to be linear and therefore, plotting the formation's temperature profile can be done with minimum input parameters such as:

- Geothermal gradient

- Total depth
- Surface temperature

5.2 Drilling Fluid Temperature

The process of drilling fluid circulation inside the wellbore involves three stages,

1. Fluid enters the drillpipe at surface and moves down the conduit
2. At the bottomhole, fluid leaves the drillpipe and enters the annulus
3. Fluid moves up the annulus and exits the conduit at surface

This process is illustrated in Figure 5.1 below.

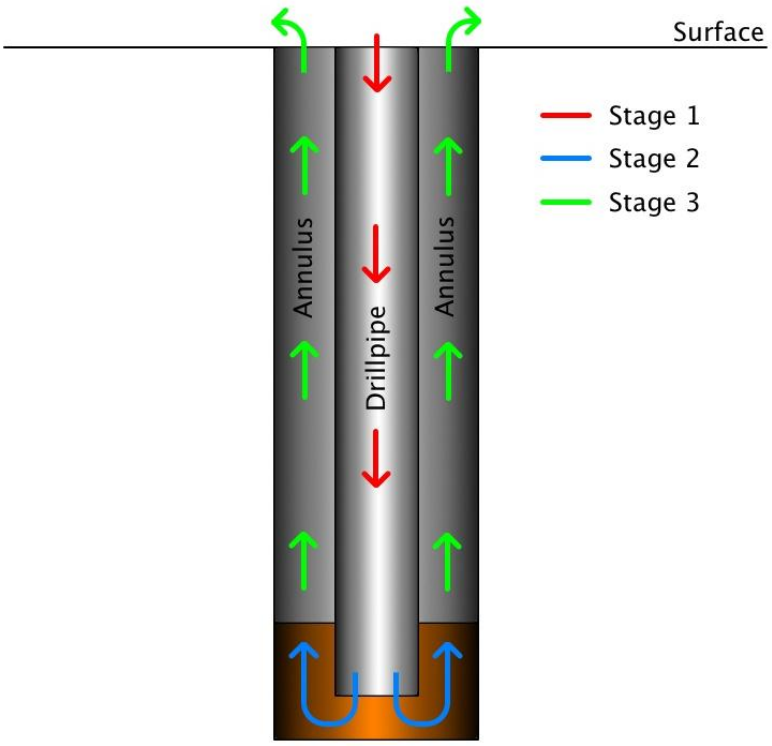

Figure 5.1: Circulation stages inside the wellbore

5.3 Heat Transfer (Analytical)

Heat transfer can be simply expressed mathematically by the following equation,

$$q = mC\Delta T \tag{5.2}$$

Note that the polarity of the terms defines the direction of heat flow, which, by convention, a positive term refers to heat gain whilst a negative term means heat loss.

By taking into account the process of drilling fluid circulation as described in Section 5.2, heat transfer can be modeled by solving equations both analytically and numerically.

5.3.1 First Stage: Drillpipe

During the first stage, the temperature of drilling fluid is determined by the heat transfer by convection along the drillpipe, $q_{d(z)}$, exchange of heat via conduction between the drillpipe and the annulus, $q_{a\to d}$, and time. By taking these heat flows into mathematical context, an analytical model can be developed, which is as follows,

$$\begin{aligned} q_{d(z)} &= mC_{fl}T_d\big|_z \\ q_{d(z+\Delta z)} &= mC_{fl}T_d\big|_{z+\Delta z} \\ q_{a\to d} &= 2\pi r_d U_d[T_a(z) - T_d(z)]dz \end{aligned} \tag{5.3}$$

Heat Balance in Drillpipe

The heat balance inside the drillpipe can be expressed by the following,

$$q_{d(z)} + q_{a\to d} = q_{d(z+\Delta z)} \tag{5.4}$$

The first two terms on the left-hand side describes the heat gain in the differential element via convection and conduction, respectively. The term on the right-hand side expresses the heat loss from the differential element through fluid flow. By substituting the equations, heat balance equation inside the drillpipe is as follows,

$$\begin{aligned} mC_{fl}T_d\big|_z + 2\pi r_d U_d[T_a(z) - T_d(z)]dz &= mC_{fl}T_d\big|_{z+\Delta z} \\ 2\pi r_d U_d[T_a(z) - T_d(z)]dz & \\ = mC_{fl}(T_d|_{z+\Delta z} - T_d|_z) & \end{aligned} \tag{5.5}$$

Rearranging,

$$mC_{fl}\frac{\delta T_d}{\delta z} - 2\pi r_d U_d[T_a(z) - T_d(z)] = 0 \tag{5.6}$$

Where,

r_d is the radius of the drillpipe (in),

U_d is the heat transfer coefficient between drillpipe and annulus,

T_a is the temperature in the annulus (°F),

T_d is the temperature in the drillpipe (°F),

m is the mass flow rate of fluid (gpm),

ρ is the density of fluid (ppg),

A is the surface area of drillpipe (in^2),

C_{fl} is the heat capacity of fluid (BTU/lb-°F),

z is the depth (ft)

The term on the left-hand-side describes the heat flow via conduction that occurs between the annulus and drillpipe as a function of depth and time. The first term on the right-hand-side describes how the temperature varies spatially i.e. in space, and the second term, temporally i.e. in time. In other words, the first term on the right-hand side expresses the accumulation of heat in the drillpipe (via convection of flowing mud). The second term defines how the temperature inside the drillpipe changes with time.

5.3.2 Second Stage: Bottomhole

The temperature of drilling fluid during the second stage, which is located at the bottomhole, is such that the fluid temperature leaving the drillpipe is equivalent to the fluid temperature entering the annulus.

Similarly, a mathematical model can be derived from the knowledge of this heat flow, which is basically,

$$T_d(z_{TD}, t) = T_a(z_{TD}, t) \tag{5.7}$$

Where,

z is the depth (ft),

TD is the total depth (ft)

5.3.3 Third Stage: Annulus

Finally, during the third stage, the mud temperature is determined by heat transfer via convection along the annulus, heat exchange via conduction between both formation and annulus, and annulus and drillpipe, and also time.

Again, from these heat exchanges, a mathematical model can be obtained which is shown in the following,

$$\begin{aligned} q_{a(z)} &= mC_{fl}T_a\big|_z \\ q_{a(z+\Delta z)} &= mC_{fl}T_a\big|_{z+\Delta z} \\ q_{a\to d} &= 2\pi r_d U_d[T_a(z) - T_d(z)]dz \\ q_{F\to a} &= 2\pi r_a U_a[T_F(z) - T_a(z)]dz \end{aligned} \tag{5.8}$$

Heat Balance in Annulus

Using conservation of energy, heat balance in the annulus can be expressed by the following equation,

$$q_{F\to a} + q_{a(z+\Delta z)} = q_{a\to d} + q_{a(z)} \tag{5.9}$$

The terms on the left-hand side of Equation 5.9 describes the heat gain in the differential element in the annulus from the formation via conduction (first term) and through bulk fluid flow via convection (second term). The first two terms on the right-hand side is where heat escapes the differential element via conduction from the annulus to the drillpipe, and via convection through bulk fluid flow, respectively. By substituting the terms from Equation 5.8, the heat balance equation inside the annulus is obtained as follows,

$$2\pi r_a U_a[T_F(z) - T_a(z)]dz + mC_{fl}T_a\big|_{z+\Delta z} = 2\pi r_d U_d[T_a(z) - T_d(z)]dz + mC_{fl}T_a\big|_z$$

$$mC_{fl}(T_a|_{z+\Delta z} - T_a|_z) = 2\pi r_d U_d[T_a(z) - T_d(z)]dz - 2\pi r_a U_a[T_F(z) - T_a(z)]dz \quad (5.10)$$

Where,

r_a is the radius of the annulus (in),

Rearranging Equation 5.10,

$$mC_{fl}\frac{\delta T_a}{\delta z} + 2\pi r_a U_a[T_F(z) - T_a(z)] - 2\pi r_d U_d[T_a(z) - T_d(z)] = 0 \quad (5.11)$$

The first two terms on the left-hand side basically describes the heat exchange between the formation and annulus, and between the annulus and drillpipe through conduction along the walls of the annulus and drillpipe. The first term on the right-hand side describes the heat loss due to fluid flow, whilst the second term describes the heat flow along the annulus via convection.

Flowing fluid temperature in the wellbore can be modeled separately for each of its flow conduit i.e. drillpipe and annulus, which is a function of the well depth and circulation rate and time. The flow of fluid, in this case, is down the drillpipe and up the annulus. The reverse flow can also be modeled according to Kabir et al [**11**], but this is not considered in this project. This forward circulation model involves energy balance i.e. heat transfer between the formation and the fluid in both conduits (drillpipe and annulus).

There are a few assumptions put in place for this model to work, which are:

- Heat transfer is steady-state in the wellbore (drillpipe and annulus)
- Transient heat transfer occurs in the formation

Transient heat transfer in the radial direction can be expressed using a partial differential equation as follows,

$$\frac{\partial T}{\partial t} = \alpha\left(\frac{\partial^2 T}{\partial r^2} + \frac{1}{r}\frac{\partial^2 T}{\partial r^2}\right) \tag{5.12}$$

The overall heat balance inside the wellbore for circulating fluid is illustrated in Figure 5.2 below.

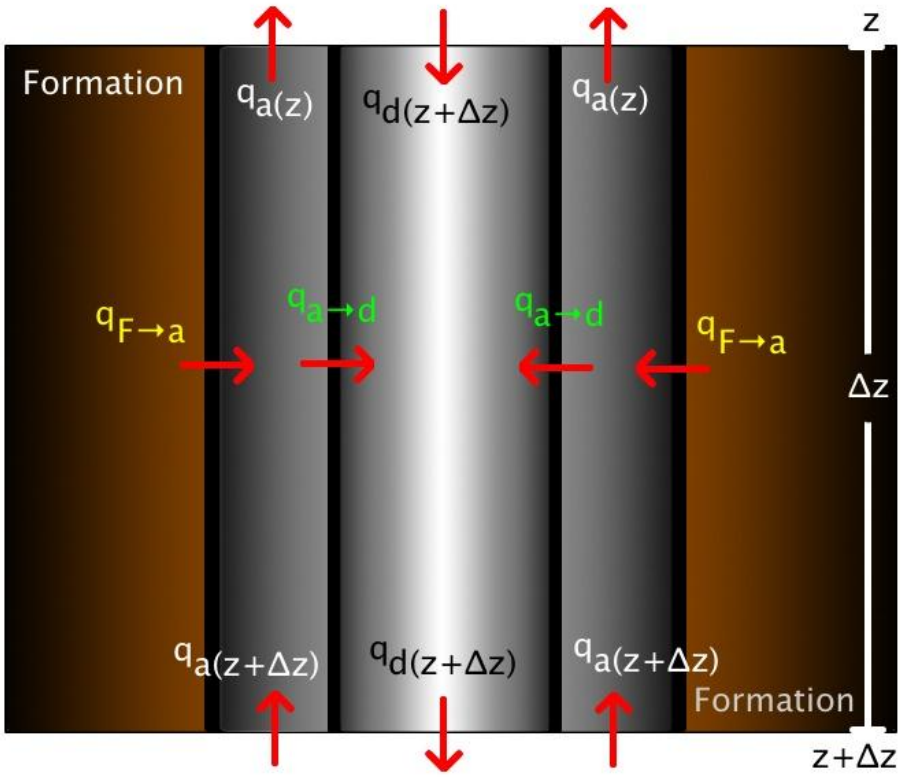

Figure 5.2: Schematic of heat flow inside the wellbore for circulating fluid

5.4 Heat Transfer (Numerical)

One of the methods to solve heat transfer problem is to use finite difference technique, which involves discretization and approximation of the function as explained previously in Section 2.5.

The derivatives of heat transfer can be expressed in terms of time and space by the following approximation,

$$\left.\frac{\partial T}{\partial t}\right|_{x_t,t_{n+1/2}} \cong \frac{T_{i,n+1} - T_{i,n}}{\Delta t} \tag{5.13}$$

$$\left.\frac{\partial T}{\partial x}\right|_{x_{t+1/2},t_n} \cong \frac{T_{i,n} - T_{i-1,n}}{\Delta x} \tag{5.14}$$

The second derivatives can then be approximated by taking the differences of the first derivative, as shown in the following,

$$\begin{aligned}\left.\frac{\partial^2 T}{\partial x^2}\right|_{x_t,t_n} &\cong \frac{\left.\frac{\partial T}{\partial x}\right|_{x_{t+1/2},t_n} - \left.\frac{\partial T}{\partial x}\right|_{x_{t-1},t_n}}{\Delta x} \\ &\cong \frac{T_{i+1,n} - 2T_{i,n} + T_{i-1,n}}{(\Delta x)^2}\end{aligned} \tag{5.15}$$

5.4.1 Conservation of Energy in the Wellbore and Formation

Harris [**6**] showed that the heat exchange inside the drillpipe can be expressed using conservation of energy by the following equation,

$$\begin{aligned}&2\pi r_d U_d(z,t)[T_a(z,t) - T_d(z,t)] \\ &\qquad = mC_{fl}\frac{\partial T_d(z,t)}{\partial z} + \rho\pi r_d^2 C_{fl}\frac{\partial T_d(z,t)}{\partial t}\end{aligned} \tag{5.16}$$

Where,

r_d is the radius of the drillpipe (in),

U_d is the heat transfer coefficient between drillpipe and annulus (),

T_a is the temperature in the annulus (°F),

T_d is the temperature in the drillpipe (°F),

T_f is the temperature of the formation (°F),

m is the mass flow rate of fluid (gpm),

ρ is the density of fluid (ppg),

C_{fl} is the heat capacity of fluid (BTU/lb-°F),

z is the depth (ft)

Consequently, the equation that describes the heat transfer inside the annulus is as follows,

$$\begin{aligned} 2\pi r_a U_a(z,t)[T_F(r_a,z,t) - T_a(z,t)] \\ - 2\pi r_d U_d(z,t)[T_a(z,t) - T_d(z,t)] \\ = -mC_{fl}\frac{\partial T_a(z,t)}{\partial z} \\ + \rho\pi(r_a^2 - r_d^2)C_{fl}\frac{\partial T_a(z,t)}{\partial t} \end{aligned} \quad (5.17)$$

Where,

r_a is the radius of the annulus (in),

U_d is the heat transfer coefficient between drillpipe and annulus (),

And finally, the temperature in the formation is expressed as follows,

$$\frac{1}{r}\frac{\partial}{\partial r}\left(r\frac{\partial T_F(z,r,t)}{\partial r}\right) = \frac{1}{\alpha}\frac{\partial T_F(z,r,t)}{\partial t} \quad (5.18)$$

Where,

α is the formation transmissivity ($^{k_F}/_{\rho C_F}$),

k_F is the formation conductivity,

ρ is the formation density,

C_F is the formation heat transfer coefficient

The heat flow in the formation is assumed to only occur in the radial direction.

Between the boundary of the annulus and formation, the heat exchange is expressed by the following,

$$-2\pi r_a U_a(z,t)[T_F(z,r_a,t) - T_a(z,t)] + 2\pi r_a k_F \left[\frac{\partial T_F(z,r_a,t)}{\partial r}\right] = 2\pi r_a \Delta r \rho C_F \frac{\partial T_F(z,r_a,t)}{\partial t} \quad (5.19)$$

5.4.2 Discretization of Heat Flow Equations

A finite difference grid is developed in order to solve how the heat transfer propagates along and the formation and the wellbore.

The temperatures in the drillpipe, annulus and the formation can be expressed by the following equations,

$$T_d(z,t) = T_d(i\Delta z, n\Delta t) = (T_d)_i^n$$

$$T_a(z,t) = T_a(i\Delta z, n\Delta t) = (T_a)_i^n$$

$$T_F(z,r,t) = T_d(i\Delta z, j\Delta r, n\Delta t) = (T_d)_{i,j}^n$$

Where,

i is the depth co-ordinate,

j is the radial co-ordinate, and

n is the time co-ordinate

There are two ways to discretize the heat flow inside the wellbore; explicit or implicit finite difference technique. These are further explained in thorough details in the following.

5.5 Explicit Method

Using explicit finite difference method which have been explained in the Literature Review (See Section 2.5.1), the heat exchange inside the drillpipe, Equation 5.16, can be discretized as follows,

$$2\pi r_d U_d \left[\frac{(T_a)_i^n + (T_a)_{i-1}^n}{2} - \frac{(T_d)_i^n + (T_d)_{i-1}^n}{2}\right] = mC_{fl}\left[\frac{(T_d)_i^n - (T_d)_{i-1}^n}{\Delta z}\right] + \rho\pi r_d^2 C_{fl}\left[\frac{(T_d)_i^{n+1} - (T_d)_i^n}{\Delta t}\right] \quad (5.20)$$

The next step is to rearrange Equation 5.20 such that the unknown term, $(T_d)_i^{n+1}$, is on the left-hand side, while the rest of the known terms on the right-hand side of the equation, as follows,

$$\begin{aligned}(T_d)_i^{n+1} &= \frac{U_d\Delta t}{\rho r_d C_{fl}}(T_a)_{i-1}^n + \frac{U_d\Delta t}{\rho r_d C_{fl}}(T_a)_i^n \\ &\quad - \frac{U_d\Delta t}{\rho r_d C_{fl}}(T_d)_{i-1}^n - \frac{U_d\Delta t}{\rho r_d C_{fl}}(T_d)_i^n \\ &\quad + \frac{m\Delta t}{\rho\pi r_d^2 \Delta z}(T_d)_{i-1}^n - \frac{m\Delta t}{\rho\pi r_d^2 \Delta z}(T_d)_i^n \\ &\quad + (T_d)_i^n \\ &= \frac{U_d\Delta t}{\rho r_d C_{fl}}(T_a)_{i-1}^n + \frac{U_d\Delta t}{\rho r_d C_{fl}}(T_a)_i^n \\ &\quad + \left[\frac{\Delta t}{\rho\pi r_d^2 C_{fl}\Delta z}\left(mC_{fl} - U_d\pi r_d \Delta z\right)\right](T_d)_{i-1}^n \\ &\quad + \Big[1 \\ &\quad - \frac{\Delta t}{\rho\pi r_d^2 C_{fl}\Delta z}\left(mC_{fl} - U_d\pi r_d \Delta z\right)\Big](T_d)_i^n \end{aligned} \quad (5.21)$$

Similarly, Equation 5.17, which describes the heat exchange inside the annulus, can be discretized for the purpose of solving using a finite difference technique as shown below,

$$2\pi r_a U_a(z,t)\left[\frac{(T_F)_i^n + (T_F)_{i-1}^n}{2} - \frac{(T_a)_i^n + (T_a)_{i-1}^n}{2}\right]$$
$$- 2\pi r_d U_d(z,t)\left[\frac{(T_a)_i^n + (T_a)_{i-1}^n}{2}\right.$$
$$\left. - \frac{(T_d)_i^n + (T_d)_{i-1}^n}{2}\right]$$
$$= -mC_{fl}\left[\frac{(T_a)_i^n - (T_a)_{i-1}^n}{\Delta z}\right]$$
$$+ \rho\pi(r_a^2 - r_d^2)C_{fl}\left[\frac{(T_a)_i^{n+1} - (T_a)_i^n}{\Delta t}\right] \quad (5.22)$$

Again, Equation 5.22 can be rearranged such that the known and the unknown terms are on the opposite side of the equation. Likewise, the only unknown term in this explicit method is $(T_d)_i^{n+1}$ whilst the rest, $(T_F)_i^n$, $(T_F)_{i-1}^n$, $(T_a)_i^n$, $(T_a)_{i-1}^n$, $(T_d)_i^n$ and $(T_d)_{i-1}^n$ are known. This is shown in the following,

$$
\begin{aligned}
(T_d)_i^{n+1} = {} & \frac{r_a U_a \Delta t}{\rho(r_a^2 - r_d^2)C_{fl}}(T_F)_{i-1}^n + \frac{r_a U_a \Delta t}{\rho(r_a^2 - r_d^2)C_{fl}}(T_F)_i^n \\
& + \frac{r_p U_p \Delta t}{\rho(r_a^2 - r_d^2)C_{fl}}(T_d)_{i-1}^n \\
& + \frac{r_d U_d \Delta t}{\rho(r_a^2 - r_d^2)C_{fl}}(T_d)_i^n \\
& - \frac{r_a U_a \Delta t}{\rho(r_a^2 - r_d^2)C_{fl}}(T_a)_{i-1}^n \\
& - \frac{r_d U_d \Delta t}{\rho(r_a^2 - r_d^2)C_{fl}}(T_a)_{i-1}^n \\
& - \frac{m \Delta t}{\rho\pi(r_a^2 - r_d^2)}(T_a)_{i-1}^n \\
& - \frac{r_a U_a \Delta t}{\rho(r_a^2 - r_d^2)C_{fl}}(T_a)_i^n \\
& - \frac{r_d U_d \Delta t}{\rho(r_a^2 - r_d^2)C_{fl}}(T_a)_i^n \\
& + \frac{m \Delta t}{\rho\pi(r_a^2 - r_d^2)}(T_a)_i^n + (T_a)_i^n \\
= {} & \frac{r_a U_a \Delta t}{\rho(r_a^2 - r_d^2)C_{fl}}(T_F)_{i-1}^n + \frac{r_a U_a \Delta t}{\rho(r_a^2 - r_d^2)C_{fl}}(T_F)_i^n \\
& + \frac{r_p U_p \Delta t}{\rho(r_a^2 - r_d^2)C_{fl}}(T_d)_{i-1}^n + \frac{r_d U_d \Delta t}{\rho(r_a^2 - r_d^2)C_{fl}}(T_d)_i^n \\
& - \frac{\Delta t\left(\pi r_a U_a \Delta z + \pi r_d U_d \Delta z + m C_{fl}\right)}{\rho\pi(r_a^2 - r_d^2)C_{fl}\Delta z}(T_a)_{i-1}^n \\
& + \left[1 - \frac{\Delta t\left(\pi r_a U_a \Delta z + \pi r_d U_d \Delta z - m C_{fl}\right)}{\rho\pi(r_a^2 - r_d^2)C_{fl}\Delta z}\right](T_a)_i^n
\end{aligned}
\tag{5.23}
$$

The issue with explicit finite difference technique is the accuracy of the approximation as it has time step limitations i.e. if the time step Δt is too big, the prediction of the numerical solution can become unstable. Furthermore, the more refined the grid is i.e. smaller Δz, the more accurate the approximation is. This may take a long time to calculate.

5.6 Implicit Method

We now look into implicit finite difference technique in order to solve this heat flow in the wellbore problem. In this case, Crank-Nicolson solution is being utilized because this method is unconditionally stable. A tridiagonal system of linear algebraic equations can be formed, which can be solved simultaneously. Equation 5.16 (heat transfer in the drillpipe) is now discretized using the θ method as follows,

$$\begin{aligned} 2\pi r_r U_d \theta[(T_a)_i^{n+1} - (T_d)_i^{n+1}] & \\ + 2\pi r_d U_d (1-\theta)[(T_a)_i^n - (T_d)_i^n] & \\ = mC_{fl}\left\{\theta\left[\frac{(T_d)_{i+1}^{n+1} - (T_d)_{i-1}^{n+1}}{2\Delta z}\right]\right. & \\ \left. + (1-\theta)\left[\frac{(T_d)_{i+1}^{n} - (T_d)_{i-1}^{n}}{2\Delta z}\right]\right\} & \\ + \rho\pi r_d^2 C_{fl}\left[\frac{(T_d)_i^{n+1} - (T_d)_i^n}{\Delta t}\right] & \end{aligned} \tag{5.24}$$

Then, Equation 5.24 can be rearranged such that the left-hand side contains the unknown terms while the rest of the known terms on the right-hand side of the equation as follows,

$$\begin{aligned} -mC_{fl}\theta(T_d)_{i-1}^{n+1} + \left[2\pi r_d U_d \theta + \frac{\rho\pi r_d^2 C_{fl}}{\Delta t}\right](T_d)_i^{n+1} & \\ + \frac{mC_{fl}\theta}{2\Delta z}(T_d)_{i+1}^{n+1} & \\ = \frac{mC_{fl}(1-\theta)}{2\Delta z}(T_d)_{i-1}^{n} & \\ + \left[\frac{\rho\pi r_d^2 C_{fl}}{\Delta t} - 2\pi r_d U_d(1-\theta)\right](T_d)_i^n & \\ - \frac{mC_{fl}(1-\theta)}{2\Delta z}(T_d)_{i+1}^{n} & \\ + 2\pi r_d U_d(1-\theta)(T_a)_i^n & \\ + 2\pi r_d U_d \theta (T_a)_i^{n+1} & \end{aligned} \tag{5.25}$$

Where,

$\theta = 0$ or 1

Notice that the final term on the right-hand side, which is an unknown temperature in the annulus. An initial guess must be made in order to solve this problem.

Similarly, heat transfer equation in the annulus (Equation 5.17) can be discretized using Crank-Nicolson method as shown below,

$$\begin{aligned} 2\pi r_a U_a \theta[(T_F)_i^{n+1} - (T_a)_i^{n+1}] \\ + 2\pi r_a U_a (1-\theta)[(T_F)_i^{n} - (T_a)_i^{n}] \\ - 2\pi r_d U_d \theta[(T_a)_i^{n+1} - (T_d)_i^{n+1}] \\ - 2\pi r_d U_d (1-\theta)[(T_a)_i^{n} - (T_d)_i^{n}] \\ = -mC_{fl}\left[\theta \frac{(T_a)_{i+1}^{n+1} - (T_a)_{i-1}^{n+1}}{2\Delta z}\right. \\ \left. + (1-\theta)\frac{(T_a)_{i+1}^{n} - (T_a)_{i-1}^{n}}{2\Delta z}\right] \\ + \rho\pi(r_a^2 - r_d^2)C_{fl}\left[\frac{(T_a)_i^{n+1} - (T_a)_i^{n}}{\Delta t}\right] \end{aligned} \quad (5.26)$$

Now rearrange Equation 5.26 to give the following,

$$\frac{mC_{fl}\theta}{2\Delta z}(T_a)_{i-1}^{n+1}+\left[2\pi r_a U_a\theta+2\pi r_d U_d\theta+\frac{\rho\pi(r_a^2-r_d^2)C_{fl}}{\Delta t}\right](T_a)_i^{n+1}-\frac{mC_{fl}\theta}{2\Delta z}(T_a)_{i+1}^{n+1}=-\frac{mC_{fl}(1-\theta)}{2\Delta z}(T_a)_{i-1}^{n}+\left[\frac{\rho\pi(r_a^2-r_d^2)C_{fl}}{\Delta t}-2\pi r_a U_a(1-\theta)-2\pi r_d U_d(1-\theta)\right](T_a)_i^{n}+\frac{mC_{fl}(1-\theta)}{2\Delta z}(T_a)_{i+1}^{n}+2\pi r_d U_d(1-\theta)(T_d)_i^{n}+2\pi r_d U_d\theta(T_d)_i^{n+1}+2\pi r_a U_a(1-\theta)(T_F)_i^{n}+2\pi r_a U_a\theta(T_F)_i^{n+1} \quad (5.27)$$

At this point, the heat flow equations in the drillpipe and annulus have been discretized, now the heat flow equation in the formation (Equation 5.18) is discretized as follows,

$$\frac{(T_F)_{i,j}^{n+1}-(T_F)_{i,j}^{n}}{\Delta t}=\frac{\alpha}{2}\left[\frac{(T_F)_{i,j-1}^{n+1}-2(T_F)_{i,j}^{n+1}+(T_F)_{i,j+1}^{n+1}}{(\Delta r)^2}+\frac{(T_F)_{i,j-1}^{n}-2(T_F)_{i,j}^{n}+(T_F)_{i,j+1}^{n}}{(\Delta r)^2}\right]+\frac{\alpha}{2}\left[\frac{1}{j\Delta r}\frac{(T_F)_{i,j+1}^{n+1}-(T_F)_{i,j-1}^{n+1}}{2\Delta r}+\frac{1}{j\Delta r}\frac{(T_F)_{i,j+1}^{n}-(T_F)_{i,j-1}^{n}}{2\Delta r}\right] \quad (5.28)$$

Rearranging Equation 5.28 gives,

$$\left[\frac{\alpha\Delta t}{4j(\Delta r)^2}-\frac{\alpha\Delta t}{2(\Delta r)^2}\right](T_F)_{i,j-1}^{n+1}+\left[1-\frac{\alpha\Delta t}{(\Delta r)^2}\right](T_F)_{i,j}^{n+1}$$
$$+\left[-\frac{\alpha\Delta t}{4j(\Delta r)^2}-\frac{\alpha\Delta t}{2(\Delta r)^2}\right](T_F)_{i,j+1}^{n+1}$$
$$=\left[-\frac{\alpha\Delta t}{4j(\Delta r)^2}+\frac{\alpha\Delta t}{2(\Delta r)^2}\right](T_F)_{i,j-1}^{n+1}$$
$$+\left[1-\frac{\alpha\Delta t}{(\Delta r)^2}\right](T_F)_{i,j}^{n+1}$$
$$+\left[\frac{\alpha\Delta t}{4j(\Delta r)^2}+\frac{\alpha\Delta t}{2(\Delta r)^2}\right](T_F)_{i,j+1}^{n+1} \quad (5.29)$$

5.7 Boundary Conditions

In order to solve these equations, boundary conditions must be set. At the surface, the temperature in the drillpipe is equivalent to the surface temperature of the pipe inlet. At the bottomhole, the temperature in the drillpipe is equivalent to the temperature in the annulus.

The boundary conditions can applied mathematically on this model is as follows,

At the drillpipe inlet, $i = 0$,

$$\left(T_p\right)_0^n = T_{dS}$$

Where,

T_{dS} is the temperature of fluid in the drillpipe inlet at the surface.

At the bottomhole, $i = imax$,

$$(T_d)_{imax}^n = (T_a)_{imax}^n$$

Now, a heat balance equation at the bottomhole can be derived as follows,

$$mC_{fl}[(T_d)_{imax-1} - (T)_{imax}] + 2\pi r_a U_a \frac{\Delta z}{2}[(T_F)_{imax} - (T)_{imax}] = \rho\pi r_a^2 \frac{\Delta z}{2} C_{fl} \frac{\partial T}{\partial t} \quad (5.30)$$

5.7.1 Drillpipe Boundary Conditions

In the drillpipe, $T = T_d$, Equation 5.30 can be discretized using Crank-Nicolson scheme as follows,

$$\begin{aligned} &mC_{fl}\theta[(T_d)^{n+1}_{imax-1} - (T_d)^{n+1}_{imax}] \\ &+ mC_{fl}(1-\theta)[(T_d)^{n}_{imax-1} - (T_d)^{n}_{imax}] \\ &+ \pi r_a U_a \Delta z \theta[(T_F)^{n+1}_{imax} - (T_d)^{n+1}_{imax}] \\ &+ \pi r_a U_a \Delta z (1-\theta)[(T_F)^{n}_{imax} - (T_d)^{n}_{imax}] \\ &= \rho\pi r_a^2 \frac{\Delta z}{2} C_{fl}\left[\frac{(T_d)^{n+1}_{imax} - (T_d)^{n}_{imax}}{\Delta t}\right] \end{aligned} \quad (5.31)$$

Rearranging Equation 5.31 results the following,

$$\begin{aligned} &mC_{fl}\theta(T_d)^{n+1}_{imax-1} - \left[mC_{fl}\theta + \frac{\rho\pi r_a^2 C_{fl}\Delta z}{2\Delta t}\right](T_d)^{n+1}_{imax} \\ &= -mC_{fl}(1-\theta)(T_d)^{n}_{imax-1} \\ &+ \left[mC_{fl} - \frac{\rho\pi r_a^2 C_{fl}\Delta z}{2\Delta t}\right](T_d)^{n}_{imax} \\ &- \pi r_a U_a \Delta z \theta (T_F)^{n+1}_{imax} \\ &- \pi r_a U_a \Delta z (1-\theta)(T_F)^{n}_{imax} \\ &+ \pi r_a U_a \Delta z \theta (T_a)^{n+1}_{imax} \\ &- \pi r_a U_a \Delta z (1-\theta)(T_a)^{n}_{imax} \end{aligned} \quad (5.32)$$

5.7.2 Annulus Boundary Conditions

Now in the annulus, $T = T_a$, similarly Equation 5.30 can be discretized to obtain the following,

$$
\begin{aligned}
mC_{fl}\theta\left[\left(T_p\right)_{imax-1}^{n+1}-(T_a)_{imax}^{n+1}\right] & \\
&+mC_{fl}(1-\theta)\left[\left(T_p\right)_{imax-1}^{n}-(T_a)_{imax}^{n}\right] \\
&+\pi r_a U_a \Delta z\theta[(T_F)_{imax}^{n+1}-(T_a)_{imax}^{n+1}] \\
&+\pi r_a U_a \Delta z(1-\theta)[(T_F)_{imax}^{n}-(T_a)_{imax}^{n}] \\
&=\rho\pi r_a^2\frac{\Delta z}{2}C_{fl}\left[\frac{(T_a)_{imax}^{n+1}-(T_a)_{imax}^{n}}{\Delta t}\right]
\end{aligned}
\tag{5.33}
$$

Rearranging Equation 5.33 gives,

$$
\begin{aligned}
\left[\frac{\rho\pi r_a^2 C_{fl}\Delta z}{2\Delta t}+mC_{fl}\theta+\pi r_a U_a\Delta z\theta\right](T_a)_{imax}^{n+1} & \\
&=\left[\frac{\rho\pi r_a^2 C_{fl}\Delta z}{2\Delta t}-\pi r_a U_a\Delta z\theta\right. \\
&\left.-mC_{fl}\theta\right](T_a)_{imax}^{n}+\pi r_a U_a\Delta z\theta(T_F)_{imax}^{n+1} \\
&+\pi r_a U_a\Delta z(1-\theta)(T_F)_{imax}^{n} \\
&+mC_{fl}\theta\left(T_p\right)_{imax-1}^{n+1} \\
&+mC_{fl}(1-\theta)\left(T_p\right)_{imax-1}^{n}
\end{aligned}
\tag{5.34}
$$

5.7.3 Formation Boundary Conditions

The boundary condition at the interface between the formation and the annulus can be expressed in the following equation,

$$
-k_F\frac{\partial T_F}{\partial r}+U_a T_F=U_a T_a \tag{5.35}
$$

Equation 5.35 is now discretized as follows,

$$
-k_F\frac{(T_F)_{i,1}^{n}-(T_F)_{i,-1}^{n}}{2\Delta r}+U_a(T_F)_{i,0}^{n}=U_a(T_a)_{i}^{n} \tag{5.36}
$$

Rearrange Equation 5.36 for each time step of n and n+1,

$$(T_F)_{i,-1}^{n} = \frac{2\Delta r U_a}{k_F}\left[(T_a)_i^n - (T_a)_{i,0}^n\right] + (T_F)_{i,1}^n \tag{5.37}$$

$$(T_F)_{i,-1}^{n+1} = \frac{2\Delta r U_a}{k_F}\left[(T_a)_i^{n+1} - (T_a)_{i,0}^{n+1}\right] + (T_F)_{i,1}^{n+1} \tag{5.38}$$

CHAPTER 6
ECD PREDICTION MODEL

6.1 Static Mud Density

Kutasov 1999 [**12**] presented an empirical equation of state for drilling muds and brines, which allows the prediction of fluid densities at downhole conditions, which is valid for either water or oil-based drilling fluids or brine;

$$\rho = \rho_o e^{[\alpha P + \beta(T - T_s) + \gamma(T - T_s)^2]} \tag{6.1}$$

where,

T is the temperature (°F),

P is the pressure (psig),

T is the international standard temperature (59°F or 15°C),

ρ is the fluid density (ppg),

ρ_0 is the fluid density at standard conditions (ppg),

α is the isothermal compressibility,

β and γ are constant coefficients

The coefficients for Equation 6.1 are listed in the Appendix (Table 10.1).

6.2 Compositional Model

The knowledge of drilling fluid compositions, mud density at surface conditions as well as the density of its individual liquid component at elevated conditions would allow the prediction of mud density at elevated temperature and pressure. In order to simulate the density of drilling fluid inside the wellbore, a compositional mass balance model was proposed (Peters *et al* 1990 [**13**]). The following equations derive this model.

At the surface temperature and pressure, the volume, V, and mass, M, of the drilling fluid are expressed as follows,

$$V_i = V_{oi} + V_{wi} + V_{si} + V_{ci} \tag{6.2}$$

Where,

$V_{oi}, V_{wi}, V_{si}, V_{ci}$ are the volumes of oil, water, solids and chemical components in a drilling fluid

$$M_i = \rho_{oi}V_{oi} + \rho_{wi}V_{wi} + \rho_{si}V_{si} + \rho_{ci}V_{ci} \tag{6.3}$$

Where,

$\rho_{oi}, \rho_{wi}, \rho_{si}, \rho_{ci}$ are the densities of oil, water, solids and chemical components in a drilling fluid

After the drilling mud has been exposed to the high temperature and high pressure inside the wellbore, volume changes are expected in the oil and water components of the mud. These volume changes are expressed as,

$$\Delta V = \frac{\rho_i V_i}{\rho_f} - V_i \tag{6.4}$$

Where,

ρ_f is the new density of components subject to HTHP

Since solids have low compressibility, they are assumed to have negligible volume changes when subject to these temperature and pressure. Now, a new mud volume can be modeled as,

$$V_i = V_o + \Delta V_o + V_w + \Delta V_w + V_s + V_c \tag{6.5}$$

Now, the drilling fluid density elevated at high temperature and pressure can be expressed using Equation 6.3 and Equation 6.5 as follows,

$$\rho(P,T) = \frac{\rho_{oi}V_{oi} + \rho_{wi}V_{wi} + \rho_{si}V_{si} + \rho_{ci}V_{ci}}{V_o + \Delta V_o + V_w + \Delta V_w + V_s + V_c} \tag{6.6}$$

By taking the volume of fractions of mud where the sum of volume fractions, f, of each of the component is equivalent to 1, Equation 6.6 can be expressed below,

$$\rho(P,T) = \frac{\rho_{oi}V_{oi} + \rho_{wi}V_{wi} + \rho_{si}V_{si} + \rho_{ci}V_{ci}}{V_o + \Delta V_o + V_w + \Delta V_w + V_s + V_c} \tag{6.7}$$

Substituting Equation 6.4,

$$\rho(P,T) = \frac{\rho_{oi}f_{oi} + \rho_{wi}f_{wi} + \rho_{si}f_{si} + \rho_{ci}f_{ci}}{1 + f_{oi}\left(\frac{\rho_{oi}V_{oi}}{\rho_{of}} - V_{oi}\right) + f_{wi}\left(\frac{\rho_{wi}V_{wi}}{\rho_{wf}} - V_{wi}\right)} \tag{6.8}$$

The assumption of this model is that any change in density of drilling fluid caused by temperature and pressure conditions is caused by the volumetric behavior of its fluid constituents, and also solid constituents are assumed to have negligible compressibility and thermal expansion.

6.3 Rheological Model

It is necessary to model how the rheological properties of the drilling fluid change with temperature and pressure. In this case, only Bingham-Plastic rheological model is applied.

6.3.1 Plastic Viscosity

Plastic viscosity of oil-based drilling fluids at elevated temperature and pressure can be obtained by normalizing with the viscosity of the base oil (Politte 1985 [**14**]). This is valid for any oil-based drilling fluid. This is expressed in the following equation,

$$\mu_{p(T,P)} = \mu_{ps}\frac{\mu_{o(T,P)}}{\mu_{os}} \tag{6.9}$$

Where,

$\mu_{p(T,P)}$ is the mud plastic viscosity at elevated temperature and pressure,

μ_{ps} is the mud plastic viscosity at surface conditions,

$\mu_{o(T,P)}$ is the base oil plastic viscosity at elevated temperature and pressure,
μ_{os} is the base oil plastic viscosity at surface conditions.

Politte 1985 [**14**] obtained an empirical expression of base oil viscosity as a function of temperature and pressure from the analysis of diesel oil-based drilling fluid, which is as follows,

$$\mu(T,P) = P \times (TP)^{A_0} \times 10^{\left(A_1 + A_2 T + A_3 TP + A_4 P + A_5 \rho + {}^{A_6}/_{\rho}\right)} \tag{6.10}$$

The values of constants $A_0, A_1, A_2, A_3, A_4, A_5, A_6$ can be found in Table 10.2 in the Appendix section. The value for ρ is obtained from Equation 6.13.

6.3.2 Yield Point

Yield point at elevated temperature and pressure is also evaluated. However, a rheological study (Politte 1985 [**14**]) has shown that pressure has little effect on the yield point. Therefore, pressure effect can be ignored. An empirical equation has been developed from the same analysis of diesel oil to evaluate the yield point, τ_y, which is valid for temperatures from 90 to 300°F.

$$\tau_y = \tau_{y0} \frac{B_0 + B_1 T + B_2 T^{-2}}{B_0 + B_1 T_0^{-1} + B_2 T_0^{-2}} \tag{6.11}$$

Where,
τ_{y0} is the yield point at surface conditions,
B_0, B_1, B_2 are constants

The values of these constants can be found in Table 10.3 in the Appendix section.

6.4 ECD Model

Using the compositional model to predict the mud density as explained previously (See Section 6.2). One of the main assumptions of this model is that any change in

density of drilling fluid caused by temperature and pressure conditions is due to the volumetric behavior of its fluid constituents. In most cases, oil and water are the main constituents of drilling mud. Similar to Equation 6.8, this model can be expressed by the following equation,

$$\rho_{mf} = \frac{\rho_{mi}}{1 + f_o\left(\frac{\rho_{oi}}{\rho_{of}} - 1\right) + f_w\left(\frac{\rho_{wi}}{\rho_{wf}} - 1\right)} \tag{6.12}$$

where,

ρ_{mi} is the mud density at reference condition

ρ_{mf} is the mud density at elevated temperature and pressure

ρ_{oi}, ρ_{wi} are oil and water densities at reference conditions

ρ_{of}, ρ_{wf} are oil and water densities at elevated temperature and pressure

f_o, f_w are volume fractions of oil and water

By studying the volumetric behaviour of the each of the fluid constituent, its respective density can be determined.

6.4.1 Volumetric Behaviour of Oil Phase

An empirical equation is used to describe the volumetric behavior of the oil phase, which is developed by Politte 1985 [**14**], and this equation can be expressed as the following:

$$\rho_o(\mathrm{P,T}) = C_0 + C_1 PT + C_2 P + C_3 P^2 + C_4 T + C_5 T^2 + \cdots \tag{6.13}$$

where,

T is temperature (°F),

P is pressure (psi),

$C_0, C_1, C_2, C_3, C_4, C_5$ are constants with the following values,

The values of these constants can be found in Table 10.4 in the Appendix.

6.4.2 Volumetric Behaviour of Water Phase

Politte 1985 [**14**] also developed another empirical equation to describe the volumetric behavior of the water phase as follows:

$$\rho_w(\mathrm{P,T}) = D_0 + D_1 T + D_2 P \tag{6.14}$$

Where,

T is temperature (°F),

P is pressure (psi),

D_0, D_1, D_2 are constants with the following values,

Constants values can be found in Table 10.5 in the Appendix section.

6.4.3 Evaluating Frictional Pressure Loss

As discussed previously in the Literature Review (See Section 2), in order to determine the ECD, the frictional pressure loss must first be determined in the wellbore.

Apparent Viscosity

The Bingham Plastic model can be used to calculate the apparent viscosity, separately in the drillpipe and the annulus, using the following equation,

Drillpipe,

$$\mu_a = \mu_p + \frac{6.66\tau_y d}{v} \tag{6.15}$$

Annulus,

$$\mu_a = \mu_p + \frac{5\tau_y d}{v} \tag{6.16}$$

Frictional Pressure Loss

Reynolds equation (Equation 2.1) can be used to determine whether the flow is laminar or turbulent. The flow is classified as laminar when the calculated Reynolds number is equivalent to or less than 2100 (Heriot-Watt University 2005 [**4**]).

$$N_{RE} = \frac{928\rho\bar{v}d}{\mu_a}$$

If this is the case, the frictional pressure loss in each drillpipe and annulus, can be evaluated using the following equations,

Drillpipe,

$$\Delta P_f = \left(\frac{\mu_p \overline{v}}{1500d^2} + \frac{\tau_y}{225d}\right)\Delta L \tag{6.17}$$

Annulus

$$\Delta P_f = \left(\frac{\mu_p \overline{v}}{1000(d_2 - d_1)^2} + \frac{\tau_y}{200(d_2 - d_1)}\right)\Delta L \tag{6.18}$$

Where,

d_1 is the inner annular wall (in)

d_2 is the outer annular wall (in)

If the flow is classified as turbulent (for Reynolds number > 2100), the fanning friction factor, f, is calculated using Colebrook Equation which is expressed in the following,

$$\frac{1}{\sqrt{f}} = 4\log_{10}\left(N_{Re}\sqrt{f}\right) - 0.395 \tag{6.19}$$

Equation 2.7 is then used to calculate the frictional pressure loss for turbulent flow, which is as follows,

$$\Delta P_f = \frac{2f\rho v^2}{d}\Delta L$$

6.5 Evaluating ECD

As discussed in the Literature Review (see Section 2.4), ECD can be evaluated using Equation 2.8 which is basically the sum of the equivalent static density (ESD) and the equivalent fluid density due to pressure loss during flow.

The ESD can be found from the pressure exerted by the static mud column i.e. no circulation is taking place. The effects of temperature and pressure on the density and rheological properties of the drilling fluid must be taken into account and this is being done by evaluating the density using the compositional model (Equation 6.12). The base mud densities in this model are functions of temperature and pressure and with the circulating fluid temperatures simulated from the previous section, the temperature and pressure dependent density is now evaluated.

The pressure loss can be calculated in two ways and it depends on whether the fluid flowing in a laminar or turbulent fashion, which can be determined from Reynolds number. For the case of a laminar flow, the plastic viscosity and the yield point of the fluid can be both evaluated empirically using Equation 6.10 and Equation 6.11, combined with the recently obtained values of the temperature and pressure dependent densities. Now, using Equation 6.17 and Equation 6.18, the pressure loss in both flow conduits i.e. drillpipe and annulus, can now be evaluated.

For the case of a turbulent flow, the pressure loss can be determined directly using Equation 2.7 after calculating the friction factor from Colebrook Equation (Equation 6.19).

With that, the ECD for each depth can now be evaluated and then plotted.

CHAPTER 7
RESULTS & DISCUSSIONS

7.1 Static Density Model

Berambang-1 well used mainly oil-based muds throughout the drilling operations. Therefore, oil-based coefficients can be used from Equation 6.1.

Table 7.1: Results of density prediction using Kutasov's empirical formula

Temperature, (°F)	Pressure (psia)	ρ (ppg)		
		Measured	Calculated	Changes
122	2025	12.50	12.49	-0.01
140	3210	13.00	12.98	-0.02
158	4785	13.70	13.69	-0.01
176	6410	14.20	14.20	0.00
194	8015	14.70	14.70	0.00
212	9845	15.20	15.21	0.01
230	11770	15.70	15.72	0.02
248	14380	17.40	17.56	0.16
266	17795	19.70	19.98	0.28
284	20110	20.70	21.03	0.33

Table 7.1 shows the comparison between actual measured and calculated densities using the empirical equation. The results show that the density of mud can be predicted quite accurately up to around 12,000 psia or 230 °F. Beyond these conditions, the density calculations start to deviate away from the measured value, i.e. higher than measured values.

Therefore, this empirical model is only valid up to temperature and pressure of 12,000 psia and 230 °F respectively. Since Berambang-1 well is an HTHP well and in order to predict the fluid density in the borehole, the prediction model has to ensure that the calculated values can replicate the measured data throughout the well.

7.2 ECD Prediction Model

The prediction models were tested briefly on Macro in Microsoft Excel. Due to time constraints and the amount of learning the program involved to build such simulation model which proved to be insufficient for the time frame of this project, the numerical prediction model was generated using Microsoft Excel instead.

For every 200 ft, an average temperature and ECD values were evaluated and the results are plotted.

7.2.1 Results

The default Berambang-1 well input parameters are as follows:

Table 7.2: Input parameters from Berambang-1 well

Well Properties	
Total vertical depth, ft	19,000
Drillpipe radius, in	6
Annulus radius, in	8.5
Circulation rate, gpm	500
Circulation time, hr	10
Inlet Mud Temperature, °F	140
Mud Properties	
Density, ppg	20.74
Plastic viscosity, cp	63.0
Yield Point, lb/100ft^2	58.0
Thermal conductivity, Btu/ft-°F-hr	0.3
Specific heat capacity, Btu/lb-°F	0.4
Oil-water ratio	0.594/0.006
Formation Properties	
Geothermal gradient, °F/ft	0.011
Surface temperature, °F	83
Specific heat capacity, Btu/lb-°F	0.21
Density, g/cm^3	2.65

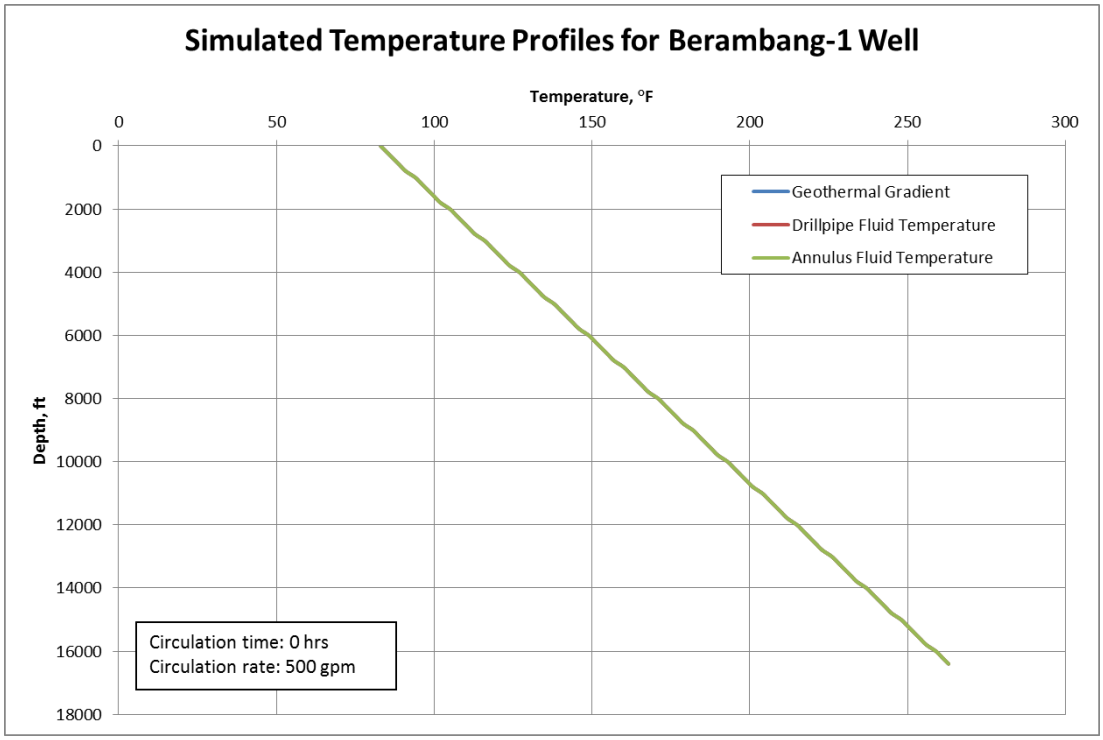

Figure 7.1: Temperature profiles during the initial stage

The initial temperature profile in the wellbore before the fluid is circulated follows the formation geothermal gradient as shown in Figure 7.1. This is a valid assumption as after circulation is halted, the temperature in the wellbore reaches equilibrium, conforming to the geothermal gradient of the formation.

This generated formation temperature profile also confirms closely to the measured data from Berambang-1 well with a bottomhole temperature of 292°F (287°F measured) at 19,000ft TVD and a geothermal gradient of 0.011°F/ft.

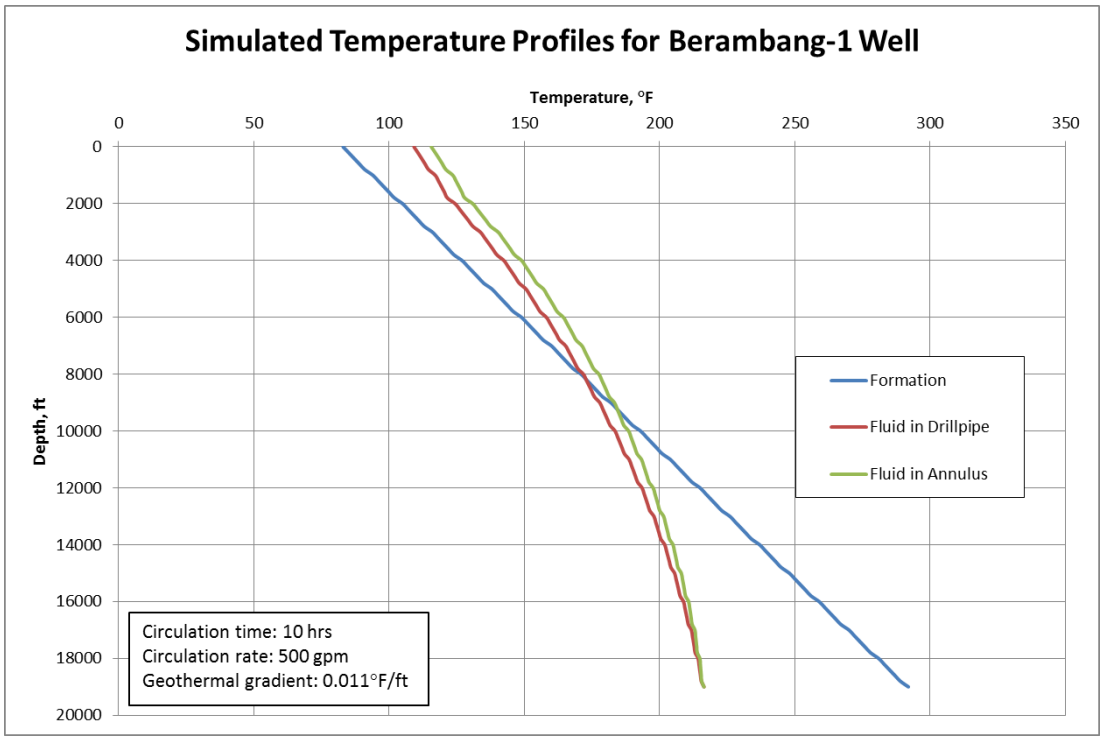

Figure 7.2: Simulated wellbore temperature profile for Berambang-1 well

Figure 7.2 shows the temperature profiles of the formation, fluid in the drillpipe as well as in the annulus after 10 hours of circulation. As seen from the figure, the flowing fluid down the drillpipe gains heat from the annulus fluid until it reaches the bottomhole. At this depth is where communication occurs between the fluids in the drillpipe and annulus. This is also where the temperatures of both fluids are equal as they are not separated by any wall or boundary and in direct contact with the formation. As the fluid enters the annulus and flow up to the surface, it loses heat energy towards the fluid in the drillpipe, which is relatively cooler.

Furthermore, the shape of the fluid temperature profile during this 10 hour circulation shows that the top-half section of the wellbore is hotter than the temperature of the formation. Whilst the bottom-half section shows how much of the bottomhole temperature has been cooled down from the circulation process. This observation confirms with the temperature trace at various depths as seen in Figure 4.1 by Raymond [**8**]. This shows the cooling effects mechanism at work by the drilling fluid, where heat is being removed from the bottom of the wellbore to the surface.

Over time, as the heat from the formation is absorbed by the fluid and circulated out to the surface, the temperature in the upper part section of the wellbore becomes higher than the formation temperature. This phenomenon observed is due to the rate at which the absorbed heat in the fluid being circulated out is faster than the rate of heat exchange between the formation and the fluids in the flow conduits. In other words, heat is being evacuated faster than it is being transferred between mediums.

At the bottomhole of depth 19,000ft, the fluid temperature has reduced to 216°F after 10 hours of circulation.

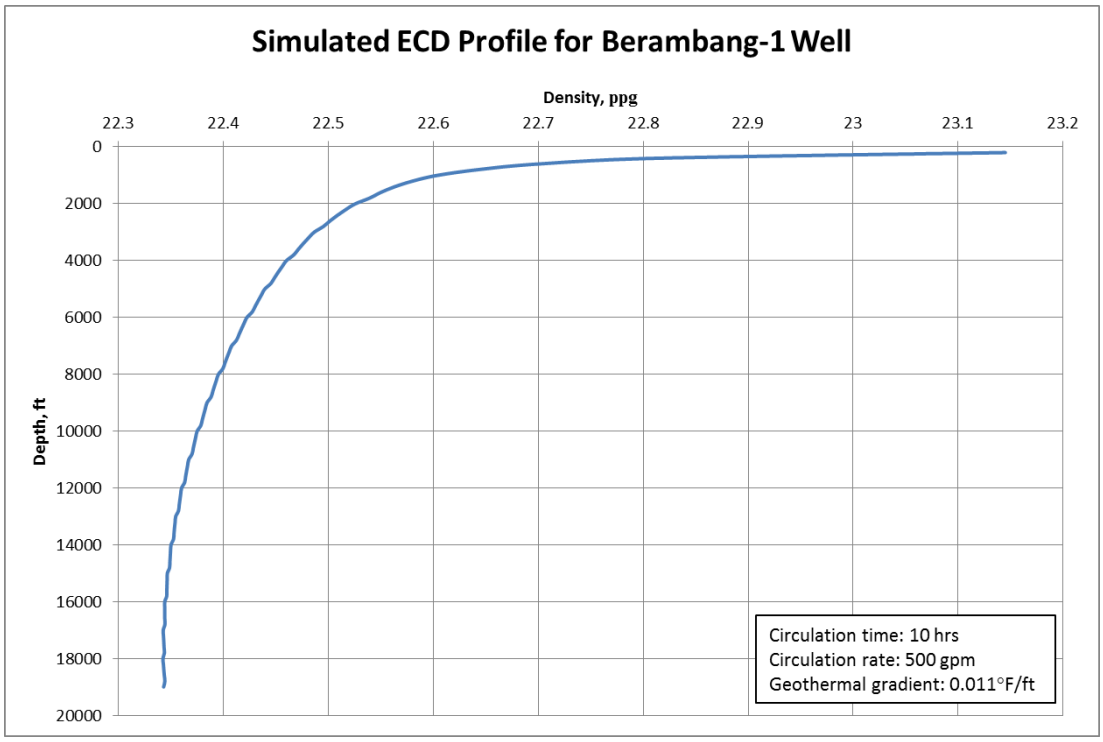

Figure 7.3: Simulated equivalent circulating density for Berambang-1 well

From the temperature profiles generated in Figure 7.2, the ECD was evaluated and plotted as shown in Figure 7.3. As seen from the results, the equivalent circulating density decreases with depth. The reason for this behaviour is that as the fluid flows down the drillpipe, the temperature increases. With increasing temperature, the fluid constituents experience thermal expansion, which consequently, reduces the ECD.

The ECD at the bottomhole is calculated to be 22.34 ppg.

7.3 Parameter Study

7.3.1 Circulation Time

Three circulation times were analyzed in 5-hour intervals, which are; initially at equilibrium (t=0 hours), after 5 hours and after 10 hours. The results of temperature profiles and ECD are plotted in Figure 7.4 and Figure 7.5.

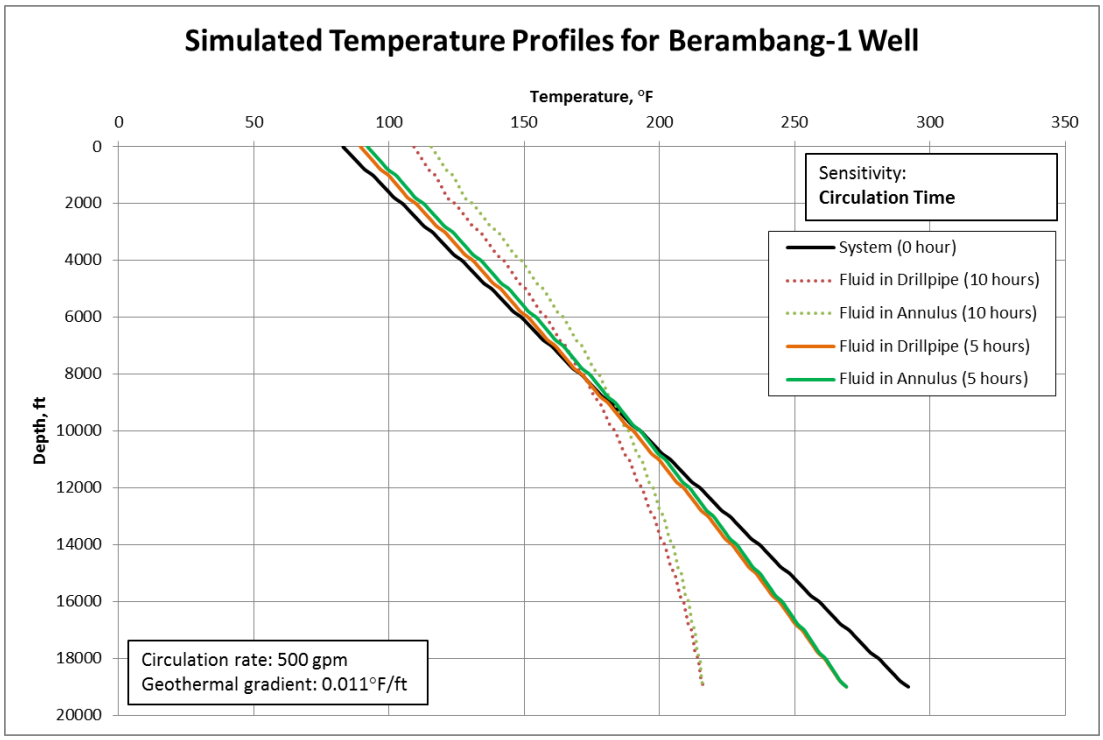

Figure 7.4: The effects of circulation time with temperature profiles

At the beginning before circulation starts, the wellbore temperature profile follows to that of the formation as the system is initially at equilibrium. After 5 hours of circulation, Figure 7.4 shows that the fluid temperatures in the wellbore start to deviate away from the geothermal gradient. The fluid temperature at the bottomhole section starts to decrease, while the upper section towards the surface, the temperature is observed to increase. After circulating for 10 hours, the temperature profile continues to follow the trend.

This observation confirms the cooling effect that occurs at the bottomhole, which reduces the temperature. While the increase in temperature in the upper section of the

wellbore is caused by circulation of fluid that carries absorbed heat from the bottomhole.

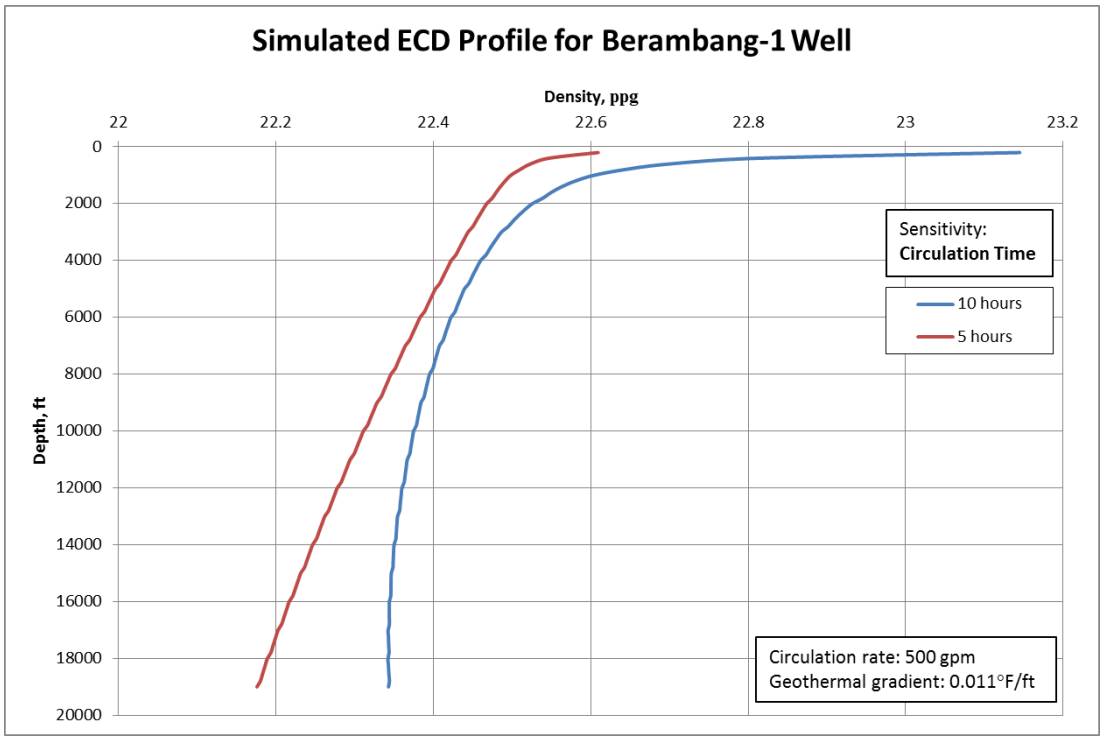

Figure 7.5: The effects of circulation time on the ECD

Figure 7.5 shows how the ECD at the bottomhole changes with circulation time. During the first 5 hours, the fluid bottomhole temperature reduces from the formation temperature. The next 5 hours, the fluid temperature continues to decrease. These observations have consequences on the ECD, where the reduction in temperature causes the fluid components to stop expanding, but rather contracting. As a result, the ECD at the bottomhole starts to increase with decreasing temperature.

7.3.2 Circulation Rates

During the study of this parameter, the circulation rate is decreased by 100 gpm from the default input rate. The temperature profiles of formation and fluid in both the drillpipe and annulus are compared between the two circulation rates. Similarly, the ECD generated from these rates are also studied.

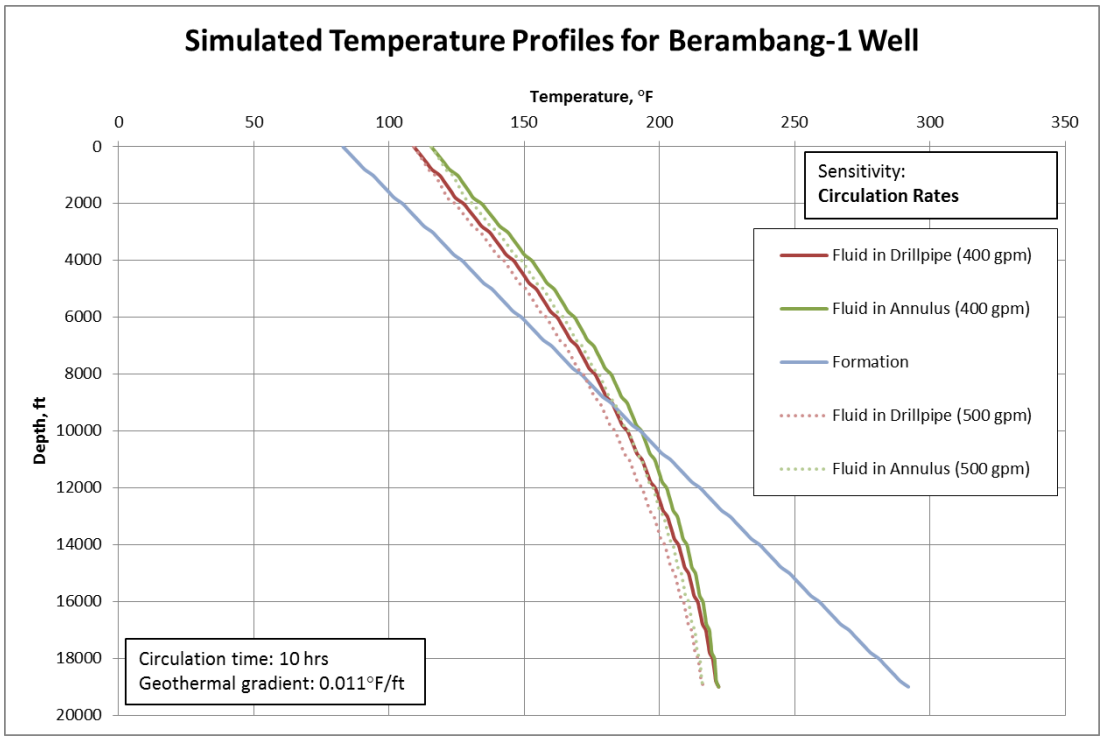

Figure 7.6: Effect of reducing circulation rates on the temperature profiles

The results, as seen in Figure 7.6, show that by reducing the circulation rate, the bottomhole fluid temperature increases. This observation is due to the declining cooling effect as the flow rate, at which the heat energy is being carried away in the circulating mud system, is reduced. Thus, this results in the slight increase in fluid temperature at the bottomhole.

For a circulation of 400gpm, the fluid temperature at bottomhole is evaluated to be 221°F.

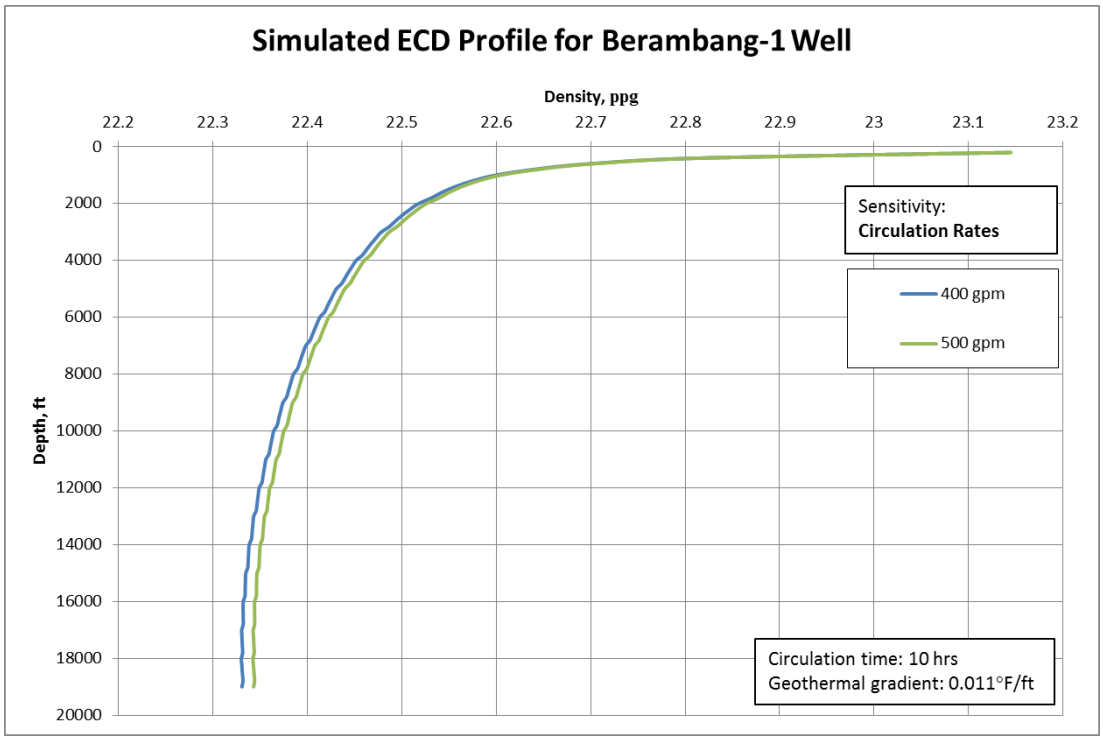

Figure 7.7: Effect of reducing circulation rates on the ECD

Figure 7.7 shows that the increased bottomhole fluid temperature due to reduction in the circulation rate has resulted the ECD at the bottomhole to decrease. This phenomenon observed is due to the effect of higher temperature that results in bigger volumetric expansions of the mud constituents and, thus, this further reduces the overall ECD at the bottomhole.

The results of this decreased circulation rate, 400gpm in this case, produced a bottomhole ECD of 22.33ppg. This reduction is ECD is, however, small and not very significant.

Increasing the circulate rates may produce the opposite result to that of reduced rates. This study, however, only takes into account laminar flow. Higher circulation rates create turbulent flow which may produce different results from this observation. This is because for turbulent flow, a different frictional pressure loss calculation (Equation 2.7) is used to compute the ECD. Compared to laminar flow where Equation 6.17 and Equation 6.18 are used to evaluate the ECD. Therefore, further study can be made to consider turbulent flow.

7.3.3 Geothermal Gradients

Geothermal gradients are increased from the input value, 0.011°F/ft to 0.016°F/ft and the fluid and formation temperature profiles as well as the ECD are compared.

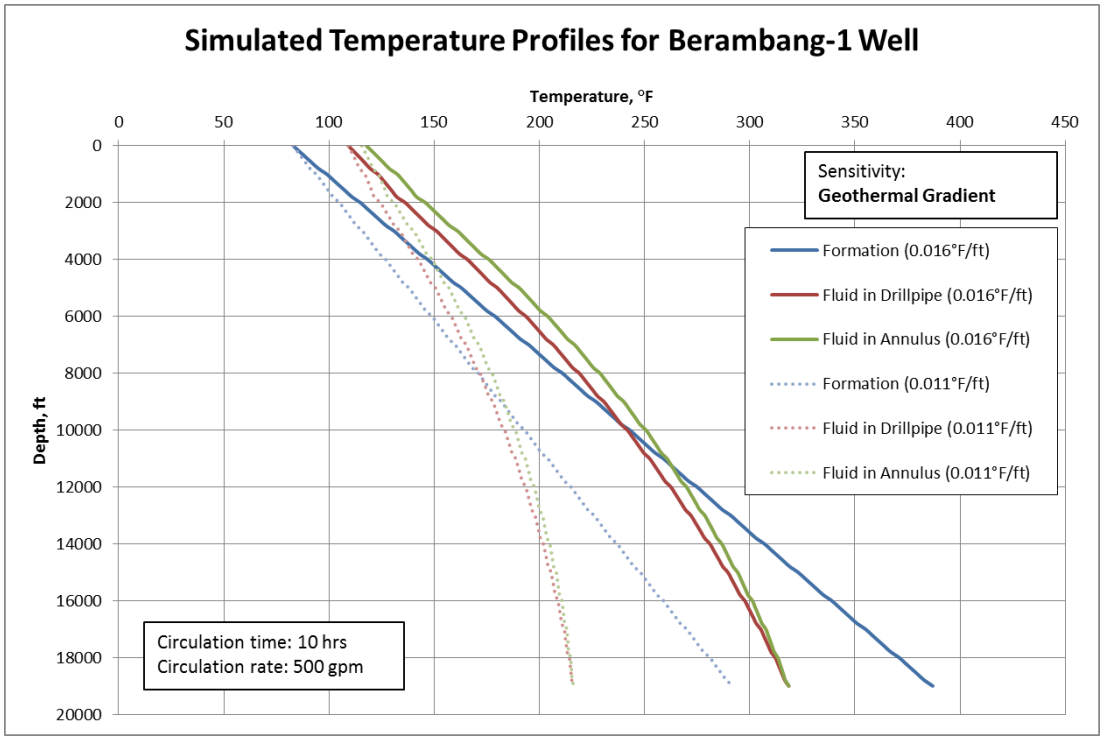

Figure 7.8: Effect of increasing geothermal gradient on the temperature profiles

Figure 7.8 shows that increasing the geothermal gradient has resulted the bottomhole circulating fluid temperature to be higher. This is as expected because as with higher geothermal gradient, the temperature increase for every foot deep is more, resulting in a much higher bottomhole formation temperature.

During circulation, cooling effects occur at the bottomhole which has resulted the wellbore to have relatively lower temperatures than the formation. Due to this difference in temperature at the bottomhole section, heat from the formation is lost to the much cooler fluid in the annulus. Furthermore, the fluid in the drillpipe is relatively cooler than that in the annulus and, hence, it gains the heat energy from this process.

The graph also shows that at higher geothermal gradient, a longer length of the wellbore is seen to have temperatures higher than the formation.

The bottomhole fluid temperature at a geothermal gradient of 0.016°F/ft is 319°F.

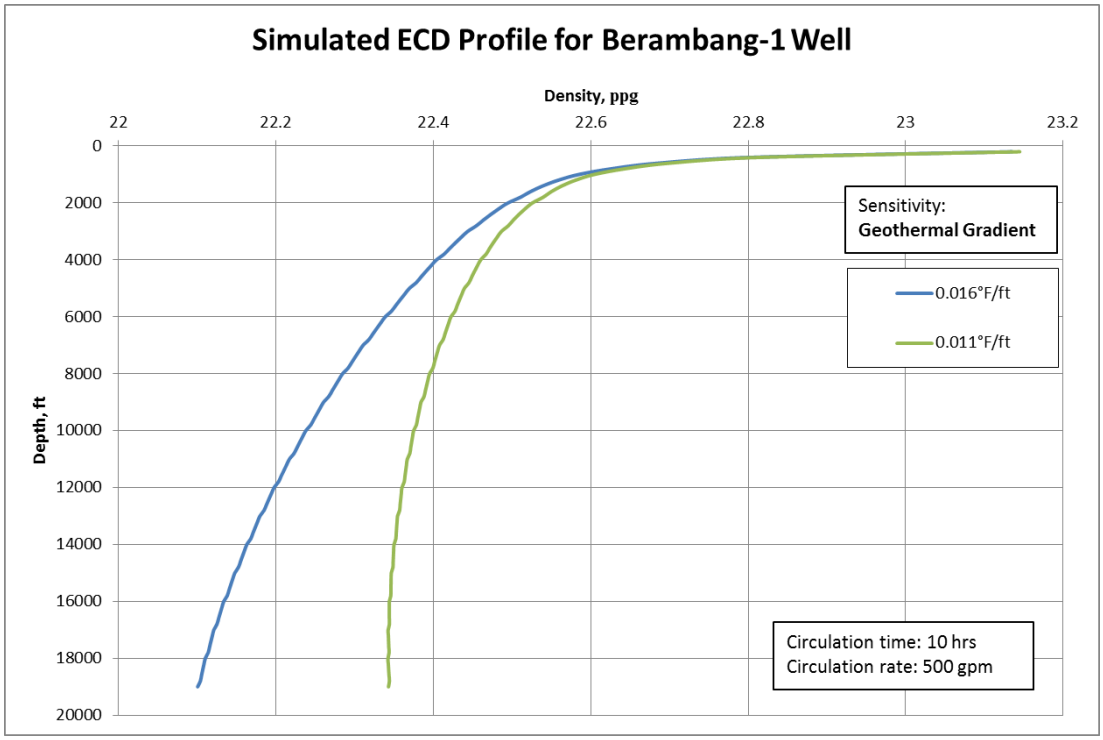

Figure 7.9: Effect of increasing geothermal gradient on the ECD

The study of the impact of increasing geothermal gradient on the ECD is shown in Figure 7.9. As discussed previously, the effect of higher geothermal gradient is that it increases the bottomhole fluid temperature. With higher temperature, it means that the bottomhole fluid experiences a much more significant thermal expansion, which consequently reduces the overall ECD as observed in the figure.

For a geothermal gradient of 0.016°F/ft, the ECD at the bottomhole has reduced to 22.10 ppg.

7.4 Sensitivity Analysis

From the three parameters studied in the previous section, a sensitivity analysis was conducted to see how the change in such parameters will affect the bottomhole circulating fluid temperature and the ECD. The value of each parameter is varied between ±30% and the results are plotted for each bottomhole temperature and ECD.

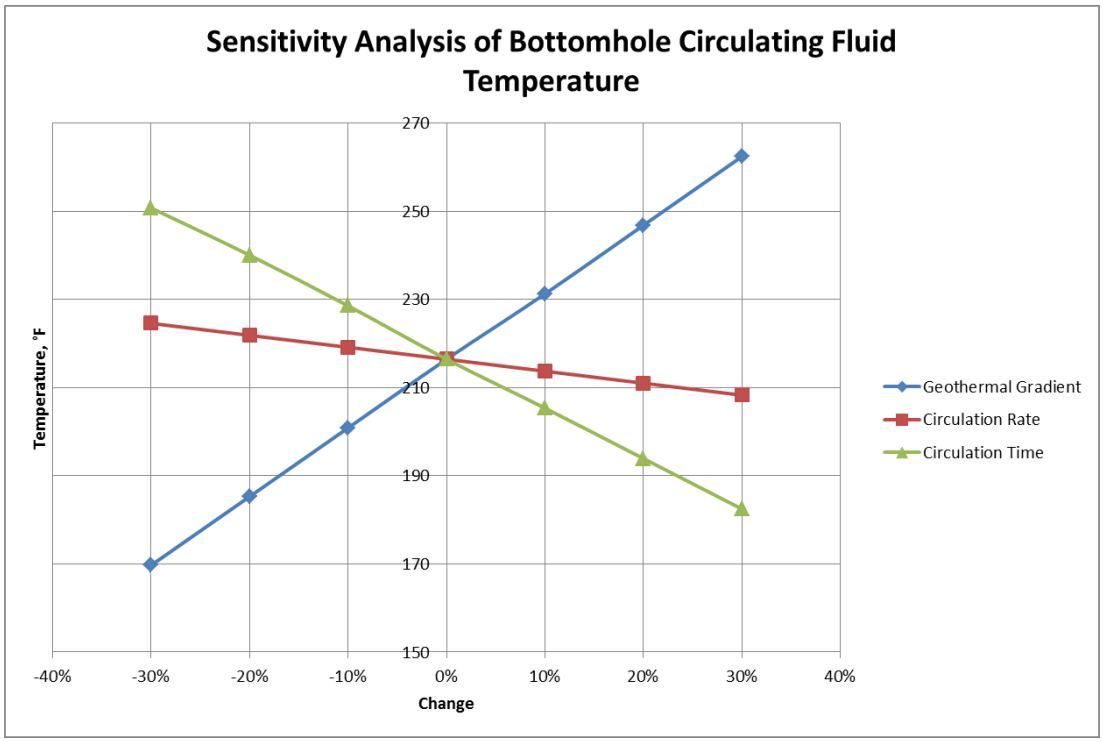

Figure 7.10: Sensitivity analysis for bottomhole circulating fluid temperature

Figure 7.10 shows how the bottomhole circulating fluid temperature varies when these three parameters are varied. Increasing geothermal gradient would cause the increase in the bottomhole temperature. The increase in both circulation rate and circulation time, however, would result a decrease in the bottomhole temperature for each case.

Out of these three parameters, the geothermal gradient seems to have the most impact on the bottomhole temperature, while the circulation rate has the least sensitive.

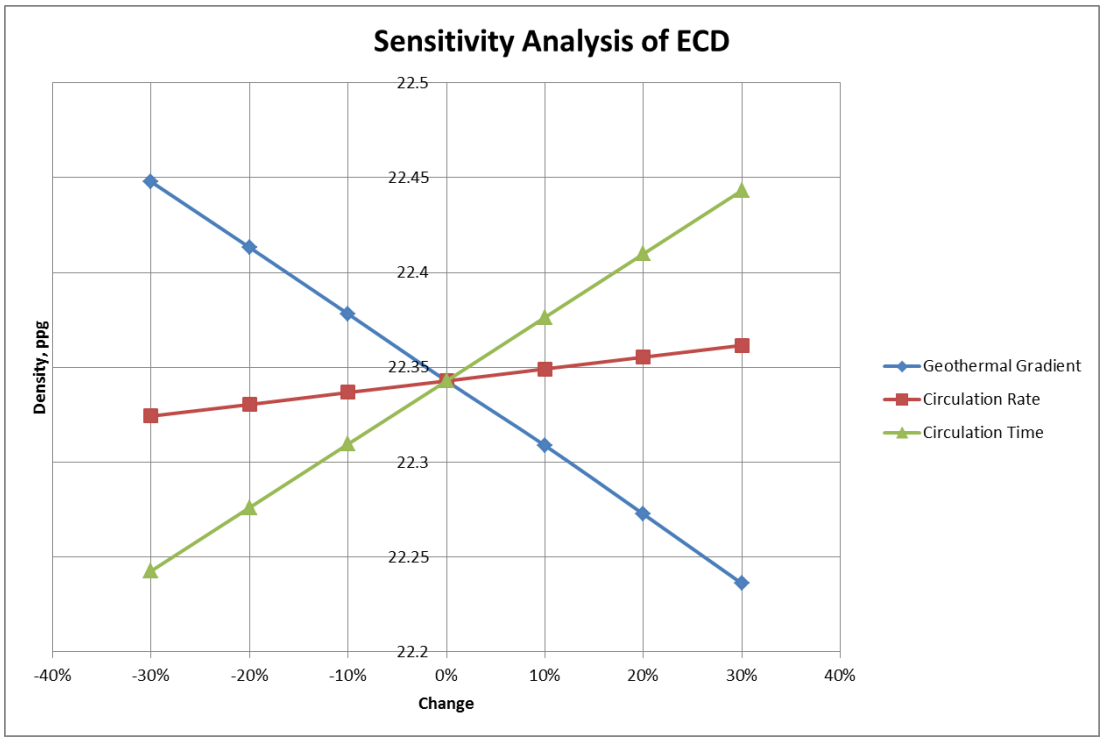

Figure 7.11: Sensitivity analysis for ECD

Similarly, Figure 7.11 now shows how these parameters affect the bottomhole equivalent circulating density. From the analysis, an increase in both the circulation rate and circulation time results in an increase in the ECD. On the contrary, the increasing geothermal gradient results in the ECD evaluated at the bottomhole to be lower.

The geothermal gradient remains the most sensitive parameter in this evaluation of ECD.

7.5 Discussions on Prediction Models

7.5.1 Temperature Model

Explicit Solution

It is shown in Section 5.5 that the fluid temperature profile in the drillpipe and annulus can be solved using the explicit method in the numerical solution. This approach, however, has several limitations.

Having a large time-step may cause the solution fail to converge, thus, the numerical approximations may become unstable. The accuracy of the approximation also depends on the size of the grid. The finer the grid, the more accurate the solution becomes but the drawback having fine grids is that the calculations can take a long time, thus, inefficient.

Crank-Nicolson Scheme

Crank-Nicolson scheme allows the numerical solutions to be approximated and the beauty of this approach is that it is unconditionally stable. This means that choosing a time step is no longer an issue. Compared to the explicit method, where choosing a time-step plays a major role ensuring a stable solution.

Applying this implicit technique requires solving a set of simultaneous equations which can be done in the matrix form.

With this technique, the prediction model should be able to simulate circulating fluid temperature profile both in the drillpipe and the annulus over a specified time, which can be specified by the user.

7.5.2 ECD Model

ECD can be determined by evaluating the circulating mud density in the wellbore as well as the frictional pressure loss. Together with the numerical approximations of the fluid temperature profile, the ECD can be modeled, thus, predicted.

Evaluating the density requires the development of a compositional model which is shown in Section 6.2, where the change in density when subjected to high temperature and pressure are due to the change in volumes of the fluids constituents in the drilling fluid. This compositional model takes into account mainly water and oil components as the rest of the solid constituents do not change very much in terms of volume and, thus, density with temperature and pressure.

7.6 Determining Well Control Issues from ECD

The results from the ECD prediction model show that during circulation, the bottomhole experiences a temperature drop with time and circulation rate. This decrease in temperature results in the cooling of the drilling fluid. During this process, the fluid constituents (mainly liquid) start to contract in volume and as a result, the overall ECD is increased.

This increase in circulating density may pose problem to the well control as HTHP formation is known to have narrow margins between the pore pressure and fracture pressure, there is a risk of fracturing the formation and thus, lost circulation.

The results of the ECD prediction model also show that the temperature increase per depth in the formation, in other words geothermal gradient, is very sensitive. This means that well control problems are further complicated with heterogeneous HTHP formations, which have non-linear geothermal gradients. This is because if the bottomhole formation has a higher geothermal gradient compared to the formation above it, the bottomhole has a higher temperature than anticipated. With higher formation temperature, the circulating fluid temperature also remains higher than expected even after the cooling effects.

High temperature causes the fluid constituents to experience thermal expansions, which consequently reduces the overall ECD. The combination of reduced ECD and narrow pore pressure and fracture pressure in HTHP formation results in the risk of formation fluid influx into the wellbore, thus, forming a kick.

CHAPTER 8
CONCLUSIONS

The outcome of this project can be ended with the following conclusions:

- HTHP wells have narrow pore pressure and fracture pressure margins, therefore it is vitally important to ensure the right mud weight and proper mud constituents selected to prevent well control problems.
- At high temperatures, components of drilling fluids degrade faster resulting mud failure where the drilling fluid unable to fulfill its primary functions.
- Crank-Nicolson scheme and Thomas algorithm are unconditionally stable and efficient for the numerical solution technique to predict fluid temperature profile in the wellbore
- Fluid density that is dependent on temperature and pressure can be evaluated using compositional model.
- Increasing circulation rates causes the bottomhole fluid temperature to decrease due to cooling effects. The same effect is seen with increasing circulation time.
- The most sensitive parameter that affects ECD is geothermal gradient. Therefore, it is important to accurately profile the formation temperature as accurately as possible, especially heterogeneous formations.
- It is possible to expect well control issues from the ECD predicted in conjunction with the pore and fracture pressure plot as well as an accurate geothermal gradient.
- Choosing the right mud constituents that can withstand high temperatures and pressures is vitally important to prevent or minimize well control issues.

8.1 Practical Applications

At the moment, an ECD prediction model does not have a practical value in terms of applications in actual drilling operations in the oil and gas industry. This is because during the drilling operations in the real world, tackling well control problems is

done by an “action-reaction” mechanism. Basically, well control issues are remedied only once they have been encountered during the operation itself.

Having an ECD prediction model that able to predict well control issues anticipated by a well, for now, is more towards educational purposes rather than industrial applications.

8.2 Recommendations

There are several things that can be pointed out of this study, which can be used to further improve the findings in the future.

8.2.1 High-Temperature Drilling Fluids

Recent HTHP wells have been utilizing invert emulsion drilling fluids which can accommodate temperatures up to 315°C (600°F).

8.2.2 Temperature Model

The temperature model outlined in this project does not take into account the water depth. The consequence of a well running through sea water would usually cause temperature to decrease at a profile. As the HTHP well data used is actually an offshore well, there are some discrepancies with the simulated geothermal gradient and, thus, fluid temperature profiles. Hence, studying this temperature effects in sea water may help improve the reliability of this prediction model.

The prediction of the fluid temperatures inside the wellbore can be further improved by taking into account the heat transfer that occurs along the drillpipe wall as well as the annulus wall (casing). This is because heat conducts faster in solid, especially metal or steel.

Further improvement of this temperature model can be made by being able to simulate fluid temperatures during other drilling operations such as tripping and workovers.

8.2.3 ECD Prediction Model

Only Bingham-Plastic rheological model is being used to create the prediction model. There is room for improvement by considering other rheological model such as Power Law and especially Herschel-Bulkley, which is widely used in the industry.

Furthermore, the prediction model is only able to calculate the ECD based on laminar flow properties. Further study can be made to understand how would the ECD change and compare during turbulent flow.

8.2.4 Sensitivity Analysis

During the prediction of fluid temperature profile in the wellbore, sensitivity analysis were carried out to study how the parameters such as circulation time, geothermal gradient, circulation rates can affect the bottomhole fluid temperatures during circulation. Further sensitivity analysis could be carried to study the effects of other input parameters such as the inlet mud temperature, thermal conductivity of mud and formation.

This sensitivity analysis can also be further expanded to understand how the volume fractions of drilling fluid components and other parameters in the ECD compositional model can affect the ECD profile.

CHAPTER 9
REFERENCES

[1] Ryan Caenn, George R. Gray, and H. C. H. Darley, *Composition and Properties of Drilling and Completion Fluids*.: Elsevier, 2011.

[2] Gunnar DeBruijn et al., "High-Pressure, High-Temperature Technologies," *Oilfield Review*, pp. 46-60, 2008.

[3] J. V. Fisk and D. E. Jamison, "Physical Properties of Drilling Fluids at High Temperatures and Pressures," *SPE*, 1989.

[4] Heriot-Watt University, *Drilling Engineering*., 2005.

[5] ASME Shale Shaker Committee, *Drilling Fluids Processing Handbook*., 2004.

[6] O. O. Harris and S. O. Osisanya, "Evaluation of Equivalent Circulating Density of Drilling Fluids Under High-Pressure/High Temperature Conditions," *SPE*, 2005.

[7] Heriot-Watt University, *Reservoir Simulation*., 2005.

[8] L. R. Raymond, "Temperature Distribution in a Circulating Drilling Fluid," *SPE-AIME*, 1969.

[9] R. Rommetveit and K. S. Bjørkevoll, "Temperature and Pressure Effects on Drilling Fluid Rheology and ECD in Very Deep Wells," *SPE*, 1997.

[10] Woha Godwin (Jnr), Joel Ogbonna, and Oriji Boniface, "Advances in Mud Design and Challenges in HTHP Wells," *SPE*, 2011.

[11] C. S. Kabir, A. R. Hasan, G. E. Kouba, and M. M. Ameen, "Determining Circulating Fluid Temperature in Drilling, Workover, and Well-Control Operations," *SPE Drilling*, pp. 74-79, June 1996.

[12] I. M. Kutasov, *Applied Geothermics For Petroleum Engineers*. USA: Elsevier,

1999.

[13] J. Ekwere Peters, E. Martin Chenevert, and Chunhai Zhang, "A Model for Predicting the Density of Oil-Based Muds at High Pressures and Temperatures," *SPE Drilling Engineering*, June 1990.

[14] M. D. Politte, "Invert Oil Mud Rheology as a Function of Temperature," *SPE*, 1985.

[15] Roland R. Sorelle, Ricardo A. Jardiolin, Peter Buckley, and John R. Barrios, "Mathematical Field Model Predicts Downhole Density Changes in Static Drilling Fluids," *SPE*, 1982.

[16] David Stiles and Mark Trigg, "Mathematical Temperature Simulators for Drilling Deepwater HT/HP Wells: Comparison, Applications, and Limitations," *SPE*, 2007.

[17] B. K. Sinha, "A New Technique To Determine the Equivalent Viscosity of Drilling Fluids Under High Temperatures and Pressures," *SPE*, 1970.

[18] Michal Spooner et al., "The Application of HTHP Water-Based Drilling Fluid on a Blowout Operation," *AADE*, 2003.

[19] Rolv Rommetveit et al., "HTHP Well Control; An Integrated Approach," *OTC*, 2003.

[20] Robert MacAndrew et al., "Drilling and Testing Hot, High-Pressure Wells," 1993.

[21] John M. Shaughnessy, Louis A. Romo, and Robert L. Soza, "Problems of Ultra-Deep High Temperature, High Pressure Drilling," *SPE*, 2003.

[22] Ron Bland, Greg Mullen, Yohnny Gonzalez, Floyd Harvey, and Marvin Pless, "HP/HT Drilling Fluid Challenges," *SPE*, 2006.

[23] Mark R. P. Tingay, Richard R. Hillis, Richard E. Swarbrick, Chris K. Morley, and Abdul Razak Damit, "Origin of Overpressure and Pore-Pressure Prediction

in the Baram Province, Brunei," *AAPG*, 2009.

[24] P. Isambourg, B. T. Anfinsen, and C. Marken, "Volumetric Behavior of Drilling Muds at High Pressure and High Temperature," *SPE*, 1996.

CHAPTER 10
APPENDICES

10.1 Introduction

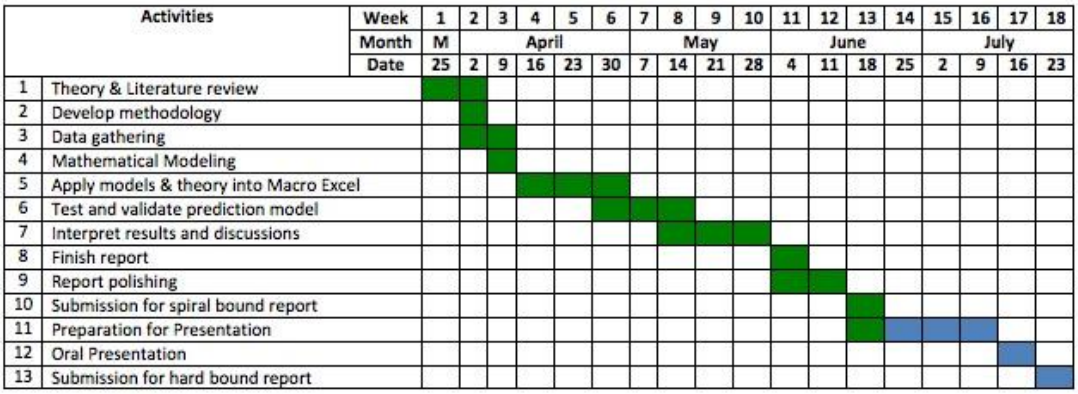

Figure 10.1: Project schedule

10.2 ECD Model Prediction

Table 10.1: Coefficients of constants for static fluid density

Mud base	ρ_0	α	β	γ
Water-base	10.770	3.3815	-2.3489	-4.2366
Water-base	13.684	3.2976	-1.7702	-5.2126
Water-base	18.079	3.0296	-1.3546	-4.4144
Oil-base	11.020	6.5146	-4.3414	1.4144
Oil-base	14.257	6.0527	-3.0027	-0.5156
Oil-base	18.049	5.1951	-2.9637	0.7460
Sodium chloride	8.591	3.9414	-1.6008	-4.5254
Sodium chloride	9.886	3.0519	-2.1967	-1.4840
Calcium bromide	15.227	1.3506	-2.4383	-0.3618

Table 10.2: Empirical constants for equation calculating base oil viscosity

$A_0 = -23.1888$	$A_1 = -0.00148$	$A_2 = -0.9501$
$A_3 = -1.9776 \times 10^{-8}$	$A_4 = 3.3416 \times 10^{-5}$	$A_5 = 14.6767$

$A_6 = 10.9973$		

Table 10.3: Empirical constants for equation calculating yield point

$B_0 = -0.186$	$B_1 = 145.054$	$B_2 = -3410.322$

Table 10.4: Empirical constants for equation calculating the volumetric behaviour of oil phase

$C_0 = 0.8807$	$C_1 = 1.5235 \times 10^{-9}$	$C_2 = 1.2806 \times 10^{-6}$
$C_3 = 1.0719 \times 10^{-10}$	$C_4 = -0.00036$	$C_5 = -5.1670 \times 10^{-8}$

Table 10.5: Empirical constants for equation calculating the volumetric behaviour of water phase

$D_0 = 8.63186$	$D_1 = -3.31877 \times 10^{-3}$	$D_2 = 2.3717 \times 10^{-5}$

Table 10.6: Bottomhole circulating fluid temperature results from sensitivity analysis

Parameters	Percentage Change						
	-30%	-20%	-10%	0%	10%	20%	30%
	Bottomhole temperatures, °F						
Geothermal gradient	170	185	201	216	231	247	262
Circulating rate	225	222	219	216	214	211	208
Circulating time	251	240	229	216	205	194	182

Table 10.7: Bottomhole equivalent circulating density from sensitivity analysis

Parameters	Percentage Change						
	-30%	-20%	-10%	0%	10%	20%	30%
	Equivalent circulating density, ppg						
Geothermal gradient	22.45	22.41	22.38	22.34	22.31	22.27	22.24
Circulation Rate	22.32	22.33	22.34	22.34	22.35	22.36	22.36
Circulation Time	22.24	22.28	22.31	22.34	22.38	22.41	22.44